Changing of the guards: detrital zircon provenance tracking sedimentological reorganization of a post-Gondwanan rift margin

Milo Barham[1], Christopher L. Kirkland[1]

[1]*School of Earth and Planetary Sciences, Centre for Exploration and Targeting – Curtin Node, the Institute for Geoscience Research (TIGeR), Curtin University, GPO Box U1987, Perth, WA 6845, Australia*

Corresponding author: milo.barham@curtin.edu.au, School of Earth and Planetary Sciences, Curtin University, GPO Box U1987, Perth, WA 6845, Australia

Running head: sediment system reorganization on a rifted margin

ACKNOWLEDGEMENTS

Pete Betts and an anonymous reviewer are thanked for their constructive comments that helped refine the paper. The authors are indebted to the Australia and New Zealand IODP Consortium for providing funding for this research, while the Oceanic Drilling Programme provided access to essential samples. We are grateful to Iluka Resources, Rohan Hine and Chris Cockburn for supplying sample NDR014 and discussions of heavy mineral recycling and sourcing. We would like to thank Bradley McDonald and Noreen Evans for assistance with LASS-ICPMS analyses, Tanya Claridge for sample processing and Kelly Merigot and Elaine Miller for support with electron microscopy. The manuscript has benefitted from discussions with Chris Elders, Mick O'Leary and Jane Cunneen. Part of this research

was undertaken using the electron microscope instrumentation (ARC LE0775553) at the John de Laeter Centre, Curtin University.

ABSTRACT

Understanding the development of sedimentary systems during continental rifting is important for tracking environmental change and lithospheric processes. Conceptual models have been developed for the sourcing, routing and facies architecture of sediments in rift-settings, driven in part by quantitative sediment tracking. Here we present laser ablation split-stream detrital zircon U/Pb geochronology and Hf-isotopes for post-rift (Cretaceous-Paleogene) clastic sediments from Ocean Drilling Program (ODP) wells and Plio-Pleistocene palaeoshoreline material, from the southern margin of Australia. Provenance results are contextualized through comparison with well-characterised source regions and regional pre- and syn-rift sediment reservoirs to track changes associated with Australia-Antarctica separation during East Gondwana break-up.

The provenance character of the post-rift sediments studied are distinct from pre-existing sediment reservoirs and demonstrate termination of previously stable sediment routing systems and a dominance of local basement of the Proterozoic Madura and Coompana provinces (~1.2 Ga and CHUR-like Hf-signatures; Moodini Supersuite) in offshore ODP wells. A composite post-rift Cretaceous?-Eocene sample in the easternmost well expresses characteristic Phanerozoic zircon age signatures associated with source regions in eastern Australia that are interpreted to reflect inversion in the Ceduna Sub-basin to the east. Detrital zircon signatures in Plio-Pleistocene palaeoshoreline sediment are also relatively distinct, indicating derivation from coastal erosion in the Leeuwin Complex (~0.5 and 0.7 Ga subchondritic grains) and Albany–Fraser Orogen (~1.2 Ga subchondritic grains) several hundred, to over a thousand kilometers to the west.

Collectively, results highlight the fundamental geological processes associated with rifting that dramatically change the character of sediment provenance via (i) isolation of pre-existing primary and secondary sources of detritus, (ii) development of new source regions in basin compartmentalized

highs and localised fault scarps, and (iii) establishment of marine and coastal currents that redefine clastic sediment transport.

Key words: long-shore drift, sediment routing, Eucla Basin, Bight Basin, Hf-isotopes, U/Pb geochronology, Ocean Drilling Program, Leg 182

INTRODUCTION

Passive margins and their rift-basin predecessors represent important sites of global hydrocarbon discovery (Lambiase et al., 1999; Mann, Gahagan, & Gordon, 2003). The sedimentary sequences that accumulate in these tectonic settings also preserve a record of the evolving environmental conditions (in particular related to the atmosphere, lithosphere and biosphere), hinterland crustal makeup and tectonic setting, across a range of scales that can help resolve details of whole Earth system processes (Armitage, Duller, Whittaker, & Allen, 2011; Barham, Kirkland, & Hollis, 2019b; Blatt & Jones, 1975; Cawood, Hawkesworth, & Dhuime, 2012; Ronov, Khain, Balukhovsky, & Seslavinsky, 1980). During the Mesozoic, new continental rifts, and eventually passive margins, were globally developed as the Atlantic, Indian and Southern Oceans opened and Pangaea broke up (Blakey, 2008; Seton et al., 2012). This rifting is thought to have radically modified sedimentary environments on a global scale (Vavrek, 2016), with Mesozoic to Cenozoic separation of Australia and Antarctica in the former East Gondwana, ending over a billion year connection between these continents (Cawood & Korsch, 2008; Huston, Blewett, & Champion, 2012; Johnson, 2013). However, limited studies have specifically explored the expression of rifting on sediment supply and routing via detrital mineral tracking despite the significance of these processes (Olierook et al., 2019).

In recent decades, advances in both the speed and precision of in situ geochronology and geochemistry have enabled analyses of detrital mineral grains to reconstruct their ultimate source regions and therefore improve understanding of denudation histories, sediment routing and depocenter connectivity (Barham et al., 2018; 2019a; Fedo, Sircombe, & Rainbird, 2003; Fielding et al., 2017;

Mason et al., 2017; Olierook et al., 2019; Xu, Snedden, Stockli, Fulthorpe, & Galloway, 2017). The mineral zircon has been most commonly analysed to constrain important source to sinks relationships due to its (i) crustal abundance, (ii) physical and chemical robustness, (iii) incorporation of U but exclusion of Pb during crystallization (excellent geochronometer), (iv) preservation of Hf- and O-isotope characteristics (ability to resolve crustal evolution and the degree of mantle input/crustal re-working), and (v) capturing of distinctive trace elements into the crystal structure (Belousova, Griffin, O'Reilly, & Fisher, 2002; Fedo et al., 2003; Grimes et al., 2007; 2015; Hawkesworth & Kemp, 2006; Roberts & Spencer, 2015). Given that the geochronological, geochemical and even grain morphological characteristics of zircon minerals from crystalline source regions are becoming well established in southern Australia, refined sediment tracking of primary and recycled components, as well as basin correlations, are becoming increasingly possible (Barham et al., 2016; 2018; 2019a; Cawood & Nemchin, 2000; Cawood, Nemchin, Freeman, & Sircombe, 2003; Haines, Wingate, & Kirkland, 2013; Lloyd et al., 2016; MacDonald et al., 2013; Makulini, Kirkland, & Barham, 2018; Olierook et al., 2019; Sircombe & Freeman, 1999; Veevers, Saeed, Belousova, & Griffin, 2005; Veevers, Belousova, & Saeed, 2016). Although the geology of East Antarctica is largely inaccessible due to ice-cover, extended Australia-Antarctica connection prior to rifting means many of the major Australian crystalline basement elements are shared with the pre-rifted adjacent Antarctic margin (Aitken et al., 2014; Fitzsimons, 2003; 2017b; Morrissey, Hand, & Kelsey, 2017a). Recent work on Proterozoic to Cenozoic depocentres around the central southern margin of Australia have increased understanding of clastic sediment dynamics in the region and shown remarkable stability of the detrital zircon fingerprint that supports extensive recycling and sustained source to sink connections for extended periods (Barham et al., 2016; 2018; Haines et al., 2016; Hou et al., 2011; Lloyd et al., 2016; MacDonald et al., 2013; Reid, Keeling, Boyd, Belousova, & Hou, 2013; Spaggiari, Kirkland, Smithies, Wingate, & Belousova, 2015; Veevers et al., 2016). New drilling campaigns and open access to Ocean Drilling Programme (ODP) legacy material provides an important opportunity to compare offshore and more marginal sediment samples against those of older depocentres. Collectively, this makes the southern margin of Australia an interesting test region to investigate the impact of continental rifting on well-established sediment systems.

This paper presents U-Pb geochronology and Hf-isotope geochemistry from detrital zircon grains recovered from late Cretaceous to Paleogene clastic units underlying Cenozoic marine carbonate sequences in ODP wells in the central Bight Basin, as well as heavy-mineral bearing coastal Plio-Pleistocene sediments (Figs. 1-2). These samples post-date complete separation of Australia and Antarctica and, when compared with published work that has demonstrated long-lived stable sediment systems for the southern central margin of Australia (Barham et al., 2018), provide important insight to changes in regional sedimentary systems as a result of Australia-Antarctica rifting and the final stage of Gondwanan break-up during an interval marking the true opening of the Southern Ocean. Furthermore, these data serve as a useful analogue for understanding changes in coastal and continental shelf sediment sourcing in response to continental break-up more broadly.

GEOLOGICAL BACKGROUND AND EVOLUTION OF THE BIGHT AND EUCLA BASINS

Crustal elements and sediment source regions

The exact nature of the basement underlying the offshore Bight Basin is constrained almost entirely through remote sensing (seismic, gravity and magnetic character) and has been sampled in few of the already limited offshore wells (including the Jerboa 1 well of the Eyre-Sub-basin; Fig. 2). The southwestern and south central margins of Australia are represented by two distinct Archean-Proterozoic cratonic blocks fringed with Proterozoic orogenic belts, which reflect reworking during protracted assembly of the Australian continent (Figs. 1-2; Betts & Giles, 2006; Cawood & Korsch, 2008; Johnson, 2013). In the southwest, the Archean Yilgarn Craton is bordered on its western margin by the late Mesoproterozoic to Cambrian Pinjarra Orogen that formed as a result of India-Australia collision and Gondwana assembly (Collins, 2003; Markwitz, Kirkland, & Evans, 2016). On its southeastern side, the Yilgarn Craton has been modified by the Palaeo-Mesoproterozoic Albany−Fraser Orogen, which developed as a result of crustal reworking and juvenile additions during amalgamation of the Archean Yilgarn and Gawler-Mawson cratons (Griffin, Belousova, Shee, Pearson, & O'Reilly, 2004; Spaggiari et al., 2015). In central Australia, Proterozoic tectono-metamorphic events with significant similarities to the Albany-Fraser Orogen are preserved in the

Musgrave Province, and demonstrate the broader docking of the Gawler-Mawson Craton with the North Australia Craton and the Yilgarn Craton component of the larger West Australian Craton (Kirkland et al., 2013; 2015). The present day expression of the Archean Gawler Craton in central South Australia is a remnant of the larger Mawson Continent that was split during Mesozoic separation of Australia and Antarctica (Belousova, Reid, Griffin, & O'Reilly, 2009; Boger, 2011; Cawood & Korsch, 2008; Kositcin, 2010a; Payne, Hand, Barovich, Reid, & Evans, 2009). Recent drilling has characterised the Palaeo-Mesoproterozoic oceanic-affinity Madura and Coompana Provinces that underlie parts of the northern and central Bight Basin (Madura Shelf) and separate the Gawler Craton, Musgrave Province and Albany-Fraser Orogen (Figs. 1-2; Fraser & Neumann, 2016; Kirkland et al., 2017; Spaggiari & Smithies, 2015). The ODP wells studied here were drilled to the east of the inferred (based on gravity) continuation of the Mundrabilla Shear Zone that separates the Madura and Coompana Provinces. However, given gravitational anomalies, it is unclear whether crystalline basement in the offshore sampling area relates to the eastern Madura or western Coompana Province. Distinctive ages of magmatic and metamorphic events in the regional crystalline basement (Table 1), can be matched to those of detrital zircon grains and used to determine their primary source regions, and thus be used as a proxy for provenance reconstructions of associated sediment.

Regional depocenter evolution

There are several distinct sedimentary basins/systems recognised through central and southern Australia that may have acted as intermediate sediment reservoirs for the clastic sediments analysed herein. Many of these depocenters initiated at sites influenced by deeper crustal structures formed during earlier tectonic events (Gibson et al., 2013; Totterdell & Bradshaw, 2004; Willcox & Stagg, 1990). Therefore, the understanding of basins, sediment-fills, crystalline source regions and tectonics on the southern margin of Australia are intimately linked.

Throughout central Australia lies the intracratonic Neoproterozoic to Palaeozoic Centralian Superbasin, which comprises sediments with a shared depositional history across the discrete depocentres of the Amadeus, Officer, Georgina, Ngalia and Murraba Basins (Grey et al., 2005; Haines

et al., 2013; 2016; Walter, Veevers, Calver, & Grey, 1995). As the largest preserved element of the Centralian Superbasin, the largely buried Officer Basin extends broadly NNW-SSE from central Australia and underlies Mesozoic sediments that formed during the rifting of Australia and Antarctica (Figs. 1-2; Barham et al., 2018; Haines, Hocking, Grey, & Stevens, 2008). Much of the later Neoproterozoic to early Palaeozoic stratigraphy of the Officer Basin reflects terrestrial environments and a significant pulse of clastic sedimentation from the adjacent central Australian Musgrave Province during the Petermann and Paterson orogenies (Fig. 1; Haines et al., 2013).

Although Palaeozoic sediments are preserved in isolated depocentres, palaeovalleys and basins fringing the onshore Cenozoic Eucla Basin, as well as underlying it (Barham et al., 2018; Bendall, Jensen-Schmidt, Holford, Dutch, & Pawley, 2016; de Broekert & Sandiford, 2005; Lowry, 1970; Reid et al., 2013), significant quantities of sediment are not recorded across the southern margin region until the Mesozoic. In the Cretaceous, the break-up of Gondwana drove the development of depocentres on the southern margin of Australia, as well as influenced the transcontinental drainage system that connected the Ceduna Sub-basin and the eastern margin of Australia (Espurt, Callot, Totterdell, Struckmeyer, & Vially, 2009; Lloyd et al., 2016; Müller, Flament, Matthews, Williams, & Gurnis, 2016; Salles, Flament, & Müller, 2017; Veevers et al., 2016). Commencing in the mid-Jurassic, fault bounded half-graben depocenters developed as Australia-Antarctica separation led to an incipient rift that propagated eastwards, ultimately leading to the broadly coastline-parallel series of basins, sub-basins and intervening platforms that constitute the magma-poor Southern Rift System (Meeuws, Holford, Foden, & Schofield, 2016; Stagg et al., 1990). The evolution from rift-perpendicular to oblique rift stresses, overlaid on a variable structural and compositional fabric of Archean to Palaeozoic basement has manifested significant complexities in basin development from the west to the far southeast along the southern Australian margin (Ball, Eagles, Ebinger, McClay, & Totterdell, 2013; Espurt et al., 2012; Gibson et al., 2013).

The Mesozoic Bight Basin, which stretches from the southwestern tip of Australia to Kangaroo Island, over 2000 km to the east (Figs. 1-2; Gibbons, Whittaker, & Müller, 2013; Stagg et al., 1990; Willcox & Stagg, 1990), is the largest component of the Southern Rift System, and itself consists of a

number of sub-basins and thin platforms including (from west to east); the Denmark Sub-basin, Bremer Sub-basin, Eyre Sub-basin, Madura Shelf, Ceduna Sub-basin, Duntroon Sub-basin, Couedic Shelf and the larger, predominantly deep-water Recherche Sub-basin (Bradshaw, Rollet, Totterdell, & Borissova, 2003; Totterdell & Bradshaw, 2004). Most relevant to this work, the Eyre Sub-basin is a perched half-graben bound to the north by an area of inferred basement and the Madura Shelf (a thin northerly onshore Cretaceous-only component of the Bight Basin; Barham et al., 2018), and to the southeast by the Ceduna Sub-basin, which preserves the thickest sequence (~15 km) of sediment on the southern margin and the largest known delta system in Australia (Fig. 1; Krassay & Totterdell, 2003; MacDonald et al., 2013). Existing knowledge of stratigraphic architecture and sediment accumulation patterns across the Bight Basin and the Eyre Sub-basin comes from an extensive (155,000 km^2 of continental shelf and upper slope of the western Great Australian Bight) 2D seismic reflection survey (Feary, Hine, James, & Malone, 2004; JNOC, 1992), as well as increasingly detailed smaller 3D surveys. Stratigraphic interpretations for the Eyre Sub-basin region have been developed from comparison with other southern margin sedimentary successions (Totterdell & Krassay, 2003), onshore sequences (Lowry, 1970) and a single borehole – Jerboa-1 – within the seismic survey (Fig. 2), located above a tilted fault block in the southern half-graben of the Eyre Sub-basin (Bein & Taylor, 1981). During the Cretaceous, subsidence became more thermally controlled with fluvio-lacustrine clastics deposited initially across the Madura Shelf and offshore basins (Barham et al., 2018; Totterdell et al., 2000; Totterdell & Krassay, 2003). Later, through the Lower Cretaceous, marine transgression led to a shift to marine glauconitic siltstones by the Albian (Barham et al., 2018; Totterdell & Krassay, 2003). Sedimentation continued through to the Maastrichtian in the Ceduna Sub-basin (MacDonald et al., 2013) but is not recorded in the later Cretaceous across the Madura Shelf and Eyre Sub-basin.

~~Post-rift, d~~During the Eocene, the onset of more rapid, post-rift ~~crustal~~ spreading and a progressively wider marine system between Australia and Antarctica gave rise to the circum-Antarctic current, global cooling, and prompted a switch to cool water carbonate deposition (Feary et al., 2004). The position of southern Australia over a dynamic topography low during the Cenozoic, and consequent

depression of the crust (Barnett-Moore, Flament, Heine, Butterworth, & Müller, 2014; Quigley, Clark, & Sandiford, 2010; Sandiford, 2007) facilitated accumulation of ~1 km of carbonates in offshore basins and 100's of metres in onshore sequences across a broad shallow shelf, effectively blanketing the pre-existing clastic sequences of the Bight Basin and making it the largest cool-water carbonate province in the world. Collectively, the Cenozoic succession of carbonates onshore and offshore has been referred to the Eucla Group (Li, James, & McGowran, 2003). As a consequence of ridge-push forces and propagation of stresses from complex plate margin interactions due to Australia's northward drift, intervals of compression and inversion along Australia's trailing southern passive margin contributed to punctuations of post-rift sediment sequences (Holford et al., 2014).

Elevated sea-levels during the Plio-Pleistocene eustatic high resulted in focused coastal erosion and the development of conspicuous planation surfaces now stranded as coastal plains - Israelite, Roe and Nundroo Plains from west to east (Fig. 2; James & Bone, 2007; Rovere et al., 2014). Following erosion of Eucla Group carbonates, these coastal plains were mantled by thin veneers of predominantly calcarenite sediments and later quartzose dunes (Roe Calcarenite on the Roe Plains and Bridgewater Formation on the Nundroo Plain).

MATERIALS AND METHODS

Wells and samples

This paper ~~deals with~~focuses on samples collected predominantly from ODP Leg 182 in the Great Australian Bight (Feary, Hine, & Malone, 1999; Feary et al., 2004), in addition to a single onshore sample from a shallow mineral sands borehole (operated by Iluka Resources) on the Plio-Pleistocene Nundroo Plain (NDR014; Figs. 2-3; Table 2). ODP Leg 182 comprised nine drill sites with the aim of understanding the cool water carbonate province on the southern margin of Australia (Feary et al., 2004). In this work we consider basal post-rift Paleogene clastic units only recovered in four of the deeper and more western wells drilled through the Eyre Terrace (1126, 1130 and 1134) and the mid continental rise further offshore (1128) in waters depths of ~500 m to ~3900 m (Figs. 2-3). The ODP

expedition identified seven unconformity-bound seismic sequences overlying the extensive Mesozoic-Cenozoic regional unconformity (Feary & James, 1998), with the oldest and often poorly temporally constrained (?Cretaceous-Eocene) basal clastic sequences being targeted herein (Fig. 3). These clastics are succeeded by a succession of Eocene through to modern carbonates considered equivalent to the limestone sequence of the onshore Eucla Basin (Li et al., 2003; Lowry, 1970).

Very limited clastic sample material was available for study, with all samples less than 1 kg in mass (Table 2). Samples from ODP wells were disaggregated using the electro-pulse SELFRAG system at the John de Laeter Centre (JdL), Curtin University. The resulting loose sediment, as well as unconsolidated sand sample NDR014, were subsequently sieved and washed to a 50-500 µm residue. Heavy mineral phases were concentrated via polytungstate-based heavy-liquid flotation and Frantz magnetic separation. Representative zircon grains from these heavy mineral concentrates were mounted in rows on double-sided tape attached to glass plates along with zircon standards. Epoxycure resin was used to embed the mounted grains to produce 25 mm diameter mounts, which were polished (to a 1 µm finish) to approximately half-grain thickness to expose internal crystal structures. Mounted grains were imaged using standard light microscopy, back-scattered electron microscopy and cathodoluminescence electron microscopy (MIRA3 VP-FESEM at the Microscopy and Microanalysis Facility, JdL; Supplementary Figure 1). Inclusions, metamict zones or grains with polyphase growth histories identified during microscopic examination were subsequently avoided during geochronological and geochemical grain analyses. Oscillatory zoned regions of grains were targeted wherever possible to obtain U–Pb igneous crystallization ages.

Zircon geochronology and Hf-isotope geochemistry

Zircon U–Th–Pb and Lu–Hf isotopic measurements were collected simultaneously using a laser ablation split stream inductively coupled plasma mass spectrometer (LA-SS-ICPMS) system housed in the GeoHistory Facility, JdL, Curtin University. The excimer laser (Resonetics S-155-LR 193 nm) spot diameter was set at 50 µm, and laser fluence was 2 J cm^{-2} with 26% attenuation, a repetition rate of 10 Hz for 30 s of total analysis time and ~60 s of total background capture. All analyses were

preceded by two cleaning pulses. The sample cell was flushed by ultrahigh purity He (0.68 $Lmin^{-1}$) and N_2 (2.8 $mLmin^{-1}$).

U–Th–Pb data were collected on an Agilent 7700x quadrupole mass spectrometer with high purity Ar as the carrier gas (flow rate 0.98 L min^{-1}). Analyses of unknowns were bracketed with primary zircon reference material 91500 (1062.4 ± 0.4 Ma; Wiedenbeck et al., 1995) to monitor and correct for mass fractionation and instrumental drift. Secondary zircon standards R33 (419.26 ± 0.39 Ma; Black et al., 2004) and GJ-1 (608.5 ± 1.5 Ma; Jackson, Pearson, Griffin, & Belousova, 2004) were used to monitor data accuracy and precision, and were corrected for mass bias and fractionation based on measured isotopic ratios of the primary reference material. All zircon ages are presented as Concordia ages, i.e., the age intercept of the weighted mean error ellipse with the concordia curve (Ludwig, 1998). During the course of this work, GJ-1 yielded weighted mean ages of 603 ± 5 Ma (MSWD = 1.9, n = 7) and 605 ± 4 Ma (MSWD = 1.3, n = 15), for analytical sessions 1 and 2 respectively, while R33 yielded weighted mean ages of 422 ± 3 (MSWD = 0.68, n = 7) and 419 ± 3 Ma (MSWD = 1.4, n = 14), for analytical sessions 1 and 2 respectively, all of which are within 2σ of the published age (see Supplementary Table A). Accepted data are defined as having a 2σ error ellipse within analytical uncertainty of Concordia (as within the error bounds of the analysis there is no evidence of Pb-loss). Lead concentration was monitored throughout the analyses, however, no ^{204}Pb was resolved above the level of detection and no common lead correction has been applied.

Lu–Hf isotopic data were collected from the same ablated volume as U–Th–Pb data on a Nu Instruments Plasma II MC-ICPMS. Measurements of ^{172}Yb, ^{173}Yb, ^{175}Lu, $^{176}Hf + Yb + Lu$, ^{177}Hf, ^{178}Hf, ^{179}Hf and ^{180}Hf were made simultaneously. Mud Tank (MT) zircon was used as the primary reference material for Hf isotope ratios, with a $^{176}Hf/^{177}Hf$ ratio of 0.282505 ± 0.000044 (Woodhead & Hergt, 2005). Corrected $^{176}Lu/^{177}Hf$ ratios were determined using the R33 zircon standard (0.001989 ± 0.000869; Black et al., 2004). 91500 (0.282306 ± 0.00004; Woodhead & Hergt, 2005), and GJ-1 (0.282000 ± 0.000005; Morel, Nebel, Nebel-Jacobsen, Miller, & Vroon, 2008) were treated as unknowns and used as secondary standards to monitor accuracy of data acquisition and processing. Secondary standards analyzed fell within 2σ error of the accepted $^{176}Hf/^{177}Hf$ values (Supplementary

Table A). Mud Tank (MT) zircon yielded a weighted average $^{176}Hf/^{177}Hf$ of 0.282508 ± 0.000013 (MSWD = 0.56, n = 23), R33 yielded 0.282734 ± 0.000014 (MSWD = 0.64, n = 19), 91500 yielded 0.282302 ± 0.000022 (MSWD = 1.9, n = 23) and GJ-1 yielded 0.282023 ± 0.000014 (MSWD = 0.76, n = 22) across both sessions. Stable $^{180}Hf/^{177}Hf$ ratios for all analysed zircon grains are well within that of the true value based on atomic weights and proportions, yielding values averaging 1.88684 ± 0.00028 and ranging between 1.88640 and 1.88984. Calculation of εHf values employs the decay constant of Scherer, Münker, and Mezger (2001) and the chondritic uniform reservoir (CHUR) values of Blichert-Toft and Albarède (1997).

Data were reduced in the UPbGeochron4 DRS in Iolite 3.4 (Paton, Hellstrom, Paul, Woodhead, & Hergt, 2011) and in-house Excel macros. Detrital zircon population ages were assessed using Isoplot 4.15 (Ludwig, 2012), with Excel macros used to produce detrital zircon age probability density plots (that incorporate analytical uncertainty; Gehrels, Valencia, & Ruiz, 2008). Kernel density plots (Vermeesch, 2012) define population age spectra based purely on the concentration of specific age analyses on a linear scale (and therefore exclude analytical uncertainty of the analysis). The generation of kernel density plots of detrital zircon age populations, and comparisons of detrital zircon age populations between samples (multidimensional scaling - MDS) were performed in the R statistical “provenance” analysis package (Vermeesch, Resentini, & Garzanti, 2016). MDS is based on dissimilarity measures derived from the Kolmogorov–Smirnov test, which investigates the null hypothesis that two distributions (in this case of detrital zircon population ages) are extracted from the same parent population, and is derived from the maximum vertical distance between sample cumulative distribution curves of grain ages..

RESULTS

Sedimentology

Sample 1128-1 was taken across a composite interval of weakly planar laminated pale-orange to pale-green highly calcareous sandstone and siltstone within a thick mudstone sequence, with deeper

sample 1128-2 taken from a more homogenous mottled pale-green, non-calcareous siltstone (Table 2). Sample 1134-2 was taken from a section of poorly sorted, calcareous, brachiopodal, oxidised glauconitic sandy granule-conglomerate. Samples 1126-1 and 1126-2 were taken from a relatively monotonous sequence of non-calcareous, organic-bearing, micaceous fine sandstone to siltstone. Finally, samples 1130-1 and 1130-2 were sourced from a similar stratigraphic level comprising relatively massive, strongly calcareous haematitic coarse sand to granules. Sample NDR014 comprised a fine, well-sorted sand with granule and small pebble-sized cemented chips.

U-Pb zircon geochronology

As a result of lithological and sample volume restrictions from limited core through basal clastic sequences, the number of analysable zircon grains were unavoidably constrained. However, data have been combined from stratigraphically adjacent samples for cores 1130, 1126 and 1128, where geochronologically and sedimentologically consistent, to provide populations that meaningfully capture major source contributors. Consequently, broad-scale inferences regarding provenance are considered significant to the interpretation of the regions geological history, especially considering the lack of other data available for similar sediments. Applying the statistics of Vermeesch (2004), concordant populations recovered from each sample give >95% confidence of having captured all components that represent, at worst, a source contributing 18% or more of the detrital cargo (at 95% confidence; NDR014 n=45 – every component contributing 10.9% or greater to the sample captured; 1130 n=38 – 12.5%; 1126 n=75 – 7.2%; 1134 n=66 – 8%; 1128 n=23 – 18.2%). Major ultimate-origin crystalline sources are therefore captured in our analysis.

The analytical results for all samples are listed in Supplementary Table B, and shown as both probability density plots (PDP) and kernel density estimate (KDE) diagrams (Fig. 4). We choose to take a conservative approach and discuss in detail analyses that are within two sigma analytical uncertainty of concordia in *conventional* space ($^{207}Pb/^{235}U$ vs. $^{206}Pb/^{238}U$; Group S). Discordant analyses as per this definition (where ages indicated by the $^{238}U/^{206}Pb$ and $^{207}Pb/^{206}Pb$ systems are not consistent within error of the analyses) are assigned to Group D. However, the distribution pattern of

$^{207}Pb/^{206}Pb$ ages for Group D mimics the broad pattern of concordant analyses, consistent with predominantly recent radiogenic Pb-loss affecting the discordant analyses (i.e. the $^{207}Pb/^{206}Pb$ ratio is unaffected by recent radiogenic-Pb loss).

NDR014

This sample yielded abundant rounded zircon grains, 50–300 μm long with aspect ratios up to 6:1. Under cathodoluminescence (CL), some grains display concentric growth zoning, which is truncated at grain edges. Other grains have rims of low CL response and some have higher CL response cores with oscillatory zoning. Surface pitting and rounding are consistent with mechanical abrasion during sedimentary transport. Sixty-five analyses were obtained from 65 zircon grains. The analyses are concordant to strongly normally discordant. Twenty analyses are assigned to Group D (Supplementary Table B). The remaining 45 analyses (Group S) range in age from 505 to 3200 Ma. The dominant age peak is centred on ~1170 Ma, with less significant peaks at ~510 Ma, ~690 Ma, ~1100 Ma and ~2640 Ma

ODP1130

This sample yielded highly rounded zircon grains, 25–300 μm long with aspect ratios up to 5:1. In CL, the grains display a wide range of internal textures including idiomorphic zonation, sector zonation and homogeneous low CL response domains and overgrowths. Sixty analyses were obtained from 60 zircon grains. The analyses are concordant to strongly normally discordant with twenty two analyses assigned to Group D and the remaining 38 analyses (Group S) ranging in age from 359 to 2828 Ma. The population is effectively unimodal with a reasonably broad ~1200 Ma peak and only minor late Palaeoproterozoic contributions.

ODP1126

This sample yielded abundant highly rounded zircon grains, 25–500 μm long with aspect ratios up to 6:1. Under CL, most grains display idiomorphic zonation. Homogeneous dark overgrowths in CL are rare. One hundred and fourteen analyses were obtained from 114 zircon grains with analyses concordant to normally discordant. Thirty nine analyses are assigned to Group D outside two sigma analytical uncertainty of concordia (Supplementary Table B). The remaining 75 analyses (Group S) range in age from 97 to 2016 Ma, with age peaks defined at 98 Ma (3 analyses), 103 Ma (4 analyses), 106 Ma (3 analyses), 555 Ma (4 analyses), 1097 Ma (3 analyses), 1131 Ma (10 analyses), 1149 Ma (11 analyses), 1197 Ma (7 analyses), 1227 Ma (5 analyses) and 1678 Ma (3 analyses). Overall, the population is polymodal with a dominant ~1150 Ma age peak and subordinate peaks at ~100 and ~600 Ma.

ODP1134

This sample yielded abundant highly rounded to angular zircon grains, 100–300 μm long with aspect ratios up to 6:1. Most grains display idiomorphic zonation under CL. Homogeneous dark overgrowths under CL are rare. Eighty two analyses were obtained from 82 zircons and analyses are concordant to normally discordant. Sixteen analyses are assigned to Group D and the remaining 66 analyses (Group S) range in age from 567 to 1705 Ma, with age peaks defined at 1097 Ma (16 analyses), 1144 Ma (25 analyses), and 1186 Ma (19 analyses). Overall, the population is effectively unimodal with a ~1100-1200 Ma peak and only minor isolated additional grain ages.

ODP1128

This sample yielded a relatively small population of rounded to angular zircon grains, 50–200 μm long with aspect ratios up to 6:1. In CL, some grains display idiomorphic zoning, others homogeneous overgrowths, and another subpopulation expresses faded sector zonation. Fifty-nine analyses were obtained from 59 zircons. Analyses are concordant to normally discordant. Thirty-six analyses are

assigned to Group D, with the remaining 23 analyses (Group S) ranging in age from 1106 to 2747 Ma. The population is polymodal with a dominant ~1200 Ma age peak and subordinate subpopulations at ~1700 and ~2650 Ma.

Zircon Hf-isotope geochemistry

Hf isotopic values are discussed that were measured simultaneously with the U-Pb age for analyses that are concordant and have $^{176}Yb/^{177}Hf$ ratio less than 0.07 (i.e. not extreme) due to the need to have both accurate age and interference correction to enable useful initial $^{176}Hf/^{177}Hf$ ratios to be calculated. Hafnium isotopic data are presented in Supplementary Table B and figure 5.

NDR014

Hf isotope analyses can be considered in terms of three broad age initial Hf components. Analyses with ages around 500 Ma cluster around CHUR, and have $^{176}Hf/^{177}Hf$ values of 0.2817-0.2820 (~ -15 εHf_i to -25 εHf_i). Analyses with ages of c. 1200 Ma range from $^{176}Hf/^{177}Hf$ values of ~0.2817 to 0.2822 (εHf_i -10 to +5). Analyses with ages of 2400-2800 Ma have $^{176}Hf/^{177}Hf$ values of ~0.2809 (-8 εHf_i).

ODP1130

Hf isotope analyses in this sample are scattered but predominantly plot along CHUR with initial Hf values ranging between minima and maxima of εHf_i -10 to εHf_i +10. A prominent zircon cluster at 1200 Ma has $^{176}Hf/^{177}Hf$ values of ~0.2817-0.2823 (εHf_i of -5 to +5).

ODP1126

Hf isotope analyses can be considered in terms of four broad age initial Hf components. Analyses with ages around 100 Ma are superchondritic and range up to 0.2830 $^{176}Hf/^{177}Hf$ (+20 εHf_i), ages

between 400 and 800 Ma are subchondritic and range down to 0.2820 $^{176}Hf/^{177}Hf$ (-20 εHf_i), whereas c. 1200 Ma analyses dominantly cluster around CHUR. Analyses with ages > 1600 Ma range from εHf_i ~ +5 to εHf_i ~-8.

ODP1134

Hf isotope analyses in this sample define one clear cluster with other younger subchondritic values and a few older dominantly superchondritic values. The main cluster is defined around 1200 Ma and ranges from $^{176}Hf/^{177}Hf$ values of 0.2819 to 0.2822 (εHf_i -6 to εHf_i +6).

ODP1128

Hf isotope analyses can be considered in terms of two broad age initial Hf components. Analyses with ages around 1200 Ma span a range from (εHf_i -4 to εHf_i +4). Analyses > 1400 Ma are dominantly subchondritic, cluster around 0.2815 $^{176}Hf/^{177}Hf$ at ~1.7 Ga and range from 0.2806-0.2811 $^{176}Hf/^{177}Hf$ at ~2.7 Ga (εHf_i -13 to εHf_i +1).

DISCUSSION

Given the paucity of volcanic activity and associated young volcanic zircon crystals on the non-volcanic rifted southern margin (Barham et al., 2019a; Direen, Borissova, Stagg, Colwell, & Symonds, 2007; 2011; Meeuws et al., 2016), it is unsurprising that the detrital zircon grains recovered do not provide especially relevant depositional age constraints for the samples (Cawood et al., 2012). Most samples yield maximum depositional ages >500 Ma, which exceed those determined from biostratigraphy and seismic stratigraphy (Table 2, Fig. 3). Sample ODP1126 provides the only exception to this, with the youngest coherent group of analyses in Group S yielding a concordia age of 97 ± 2 Ma (MSWD = 1.3; n = 3).

Principal detrital zircon age peaks identified in the post-rift southern margin samples can be confidently correlated with crystalline basement known within Australia (Table 1). Limited Archean grains, predominantly recovered from samples NDR014 and ODP1128 correlate with characteristic magmatism of the Yilgarn Craton (Fig. 4). Similar slightly subchondritic Hf isotope values are known for analysed Yilgarn Craton zircon crystals, as well as inherited Yilgarn Craton-derived crystals eroded from the Albany–Fraser Orogen (Fig. 5; Mole et al., 2014; Spaggiari et al., 2015).

Minor late Palaeoproterozoic contributions, most significant in samples ODP1130 and ODP1128 correspond most closely with characteristic ages and Hf-isotope values of the Albany–Fraser Orogen (Figs. 4-5). The greatest component of all samples overlap in age (~1.1-1.3 Ga) and Hf-isotopic space with zircon crystals analysed from the Madura and Coompana Provinces, the Albany–Fraser Orogen and the Musgrave Province (Table 1; Figs. 4-5). Hafnium isotope values clustering around CHUR, as well as a lack of older age components commonly associated with the Musgrave Province and Albany–Fraser Orogen, suggest that these Mesoproterozoic grains were more likely ultimately derived from the Moodini Supersuite of the Madura and Coompana Provinces (Kirkland et al., 2017). This basement is inferred to directly underlie the sampled region and to be exposed both in foot-wall fault scarps and in a Mesozoic-stripped region to the north of the Eyre Sub-basin (Figs 1-3). This interpretation may be further supported by recent studies using grain-shape characteristics to fingerprint detrital zircon sources, that suggested the Madura and Coompana Provinces were more important sediment contributors to the Madura Shelf than previously appreciated (Makulini et al., 2018).

Late Neoproterozoic and early Paleozoic zircon grains are present in sample NDR014, and despite some age overlap, are largely distinct in Hf isotope space from the broader, multiple Phanerozoic age peaks recovered in ODP1126 (Figs. 4-5). The characteristic twin age peaks (~0.5 and 0.7 Ga) in NDR014 as well as their more CHUR-like Hf-isotope values are interpreted to correspond to the Pinjarra Orogen of the Leeuwin Complex in SW Australia (Table 1; Collins, 2003; Olierook et al., 2019). The minor Phanerozoic components identified in ODP1126 more closely correspond with ages distinctive of Eastern Australia in the New England and Lachlan Orogens and Whitsunday Volcanic

Province (Bryan et al., 1997; Lloyd et al., 2016; Tucker, Roberts, Hu, Kemp, & Salisbury, 2013; 2016).

Dominant sediment routing

The age spectrum fingerprint of the stable sediment "pool" resulting from consistent routing and recycling through parts of the Officer Basin, Madura Shelf and Cenozoic shorelines fringing the onshore Eucla Basin (Barham et al., 2018; Reid et al., 2013) does not match that of the sediment examined herein (Fig. 4 & 6). Nor does the Ceduna Delta (located to the east of the study area) represent a definitive single source based on differences in the age spectra and Hf isotope values of its zircon cargo. Peak ages in the post-rift southern margin zircon populations are typically well defined, with dominant single populations indicative of substantial sourcing from known crystalline source regions (Fig. 4). Given greater polymodality to pre-existing characterised sediment reservoirs in the region, pure zircon recycling cannot explain the material examined herein (Figs. 4 & 6). No obvious sedimentological control on the provenance of the analysed post-rift clastic samples is evident either, with similar primary age and Hf-isotope characteristics seen across finer and coarser units analysed.

Hf isotope data demonstrate some overlap of ~1100-1200 Ma zircon grains from the Nundroo Plain, offshore ODP wells and Madura Shelf sediments. Unlike Madura Shelf sediments, the samples analysed herein lack a substantial sub-population of Paleoproterozoic zircon grains. The Palaeoproterozoic aged detrital grains in the post-rift sediments, have distinctly more evolved Hf isotope values than those on the Madura Shelf (Fig. 5) and are more similar to analyses from crystalline rocks in the Albany–Fraser Orogen than in the Musgrave Province. These data essentially indicate a termination of any Musgrave Province supply to more distal basin sediments post-rifting.

The possibility of recycling the dominant Mesoproterozoic zircon signature through older sedimentary successions is diminished by a lack of proximal source regions with the unimodal character expressed here. Some Neoproterozoic to Cambrian sediments from the Amadeus and Officer Basin have been shown to have similar detrital zircon age spectra dominated by an 1100-1200 Ma peak (Camacho,

Hensen, & Armstrong, 2002; Haines et al., 2016; Reid et al., 2013). However, these older sediments are likely a reflection of proximal sourcing from the Musgrave Province and, over greater distances, a more diverse zircon age spectrum typically develops.

The relatively unimodal nature of the ~1.1-1.2 Ga detrital zircon age peak in the ODP samples suggests a single dominant unadulterated sediment source, which was thus likely proximal with limited opportunity for the introduction of significant reworked sediments from adjacent reservoirs or more distal crystalline sources. The Madura and Coompana Provinces that have been identified underlying Phanerozoic basins onshore between the Yilgarn and Gawler cratons both exhibit significant crystallisation ages of 1181-1125 Ma in the Moodini Supersuite (Neumann & Fraser, 2016; Wingate, Kirkland, Spaggiari, & Smithies, 2015). Sediment cover sequences are significantly thinner overlying upthrown footwall blocks associated with the Eyre Sub-basin. Hence, it is suggested that the proximity of crystalline basement to the surface in these areas would have enabled essentially direct sourcing of sediments from the Moodini Supersuite and equivalent rocks during the late Cretaceous and early Cenozoic. Furthermore, more CHUR-like Hf-isotope signatures of detrital zircon grains in the ODP samples studied support zircon derivation from the local Madura and Coompana province basement (Fig. 5).

Breaching east-west sediment system separation

The furthest east ODP well sampled (ODP1126; Fig. 2) contains subordinate Phanerozoic zircon components that are not observed in any of the other samples analysed. These grains do not match any crystalline basement age or Hf-isotope characteristics within western or central Australia. Furthermore, detrital zircon grains like this have not previously been reported from further north in the central Bight Basin (Barham et al., 2018). Instead, age and Hf-isotope characteristics of this material demonstrate an affinity with eastern Australian crystalline sources, whose detritus is typically expressed in intermediate sediment reservoirs of the Eromanga Basin and Ceduna Sub-basin (Figs. 4-5; Lloyd et al., 2016; MacDonald et al., 2013; Tucker et al., 2016; Veevers et al., 2016). The Phanerozoic components of ODP1126 are distinguished from younger detrital zircon grains

previously identified as a volcanic component in the upper Madura Formation of the Madura Shelf (omitted from plots herein due to demonstrated exotic sourcing; Barham et al., 2016; 2018; 2019a) based on older subchondritic Phanerozoic components (characteristic in the Ceduna Delta and ODP1126) that are not equivalently expressed in the Madura Shelf material (Figs. 4-5).

Several phases of basin inversion have been identified within the Ceduna Delta from seismic data sets and elsewhere on the southern margin (Holford et al., 2014). These phases of uplift and erosion in the Ceduna Sub-basin affect sequences distinguished by detrital zircon crystallisation ages and Hf-isotope characteristics that match Phanerozoic grains within sample ODP1126 on the eastern Eyre Terrace (Lloyd et al., 2016; Macdonald, Backé, King, Holford, & Hillis, 2012; 2013). Most significantly, erosion has been noted between Palaeogene sediments (equivalent to those studied in ODP1126) and the underlying Campanian-Maastrichtian sequence (Macdonald et al., 2012). Further erosive episodes are recognised through the Cenozoic (Li et al., 2003) that lend support to being associated with relative sea-level fluctuations and ridge spreading forces inducing inversion episodes. Such inversions are interpreted to have facilitated sediment mixing across the connected shelf and enabled transfer of material from the Ceduna Delta system to the Eyre Terrace. Prior to this, substantial evidence indicates separation of sedimentary systems operating in the central northern Bight Basin (Madura Shelf) and the eastern Australian influenced Ceduna Delta (Barham et al., 2018; 2019a).

Initiation of distinct sediment routing

During Pleistocene lowstands, significant tracts (~200,000 km^2) of the shallow shelf offshore central southern Australia would have been exposed and subjected to aeolian transport mechanisms. Given the expanse of exposed sediment, dominant southwesterly winds of the Ferrell Cell and inferred dune systems developed on the shelf, dominant transport during glacial lowstands would have been from west to east (James et al., 2004).

The youngest sediment sample analysed from the Nundroo Plain (NDR014) is distinct from all major proximal sediment reservoirs (Ceduna Sub-basin, Madura Shelf and Eucla Basin Cenozoic

548 shorelines), both in terms of its zircon cargo age spectrum (lacking east coast Neoproterozoic and
549 Phanerozoic signatures, muted late Palaeoproterozoic contribution, but incorporation of distinctive ca.
550 500 and 700 Ma components) and Hf isotope profile (Figs. 4-6). Subchondritic Hf isotope data are
551 more distinctive of Mesoproterozoic detrital zircon grains from NDR014 than those of ODP samples.
552 More subchondritic values are more characteristic of the Mesoproterozoic Albany–Fraser Orogen.
553 Collectively, the geochronology and Hf-isotope data imply that NDR014 received significant detritus
554 derived from the Esperance Supersuite of the Albany–Fraser Orogen (1170 Ma peak with inherited
555 Archaean ages from the Yilgarn Craton). Although large areas of Gondwana exhibit 500-700 Ma
556 zircon grains with similar $^{176}Hf/^{177}Hf$ isotopic values (Veevers et al., 2016), the NDR014 grains of this
557 group are defined by two distinctive ~510 and ~690 Ma age peaks and fall within the envelope of Hf-
558 data available for the Leeuwin Complex of the Pinjarra Orogen (Olierook et al., 2019). These
559 subordinate late Neoproterozoic and early Paleozoic zircon grains therefore support significant
560 derivation of the sample from the west via long-shore drift and lowstand aeolian systems over ~1700
561 km. This interpretation is supported by the age spectra of detrital zircon grains from the southwestern
562 tip of Australia where the Leeuwin Complex is exposed (Augusta) and the Frankland River, which
563 drains the Albany–Fraser Orogen on the southern coast of SW Australia. Combined, these example
564 proximal sediments of the Leeuwin Complex and Albany–Fraser Orogen source regions can almost
565 entirely explain the NDR detrital population (Figs. 4 & 6).

566

567 **Implications for sediment system restructuring post-rift**

568 Comparison of the new post-rift data with pre- and syn-rift sediments from the southern margin of
569 Australia demonstrates some fundamental rift-related processes on sedimentation (Fig. 7):

570 1. The potential of pre-existing sediment reservoir isolation via rift-related subsidence.
571 Associated with accelerated rifting during the Eocene, the sea-way separating Australia and
572 Antarctica grew more rapidly (Hou, Alley, Frakes, Stoian, & Cowley, 2006). Simultaneously,
573 higher global sea-levels and a dynamic topographic low beneath the region (Barnett-Moore et
574 al., 2014), resulted in marine inundation and development of extensive carbonate deposits of

the Eucla Basin. Along with climatically induced aridity, this expansive region of karst with no surface drainage has effectively isolated the previous sediment reservoirs from offshore and modern coastal systems, preventing significant recycling of this sediment-pool despite its previous regional stability and longevity over several hundred million years (Barham et al., 2018).

2. The importance of relative uplift for enabling reworking of rift-associated sediments (Gawthorpe & Leeder, 2000). On the southern margin of Australia, basin inversion has been shown to cause reworking of intra-rift sediments, with material from ODP1126 indicating dispersion from the eastern Bight Basin (Ceduna Sub-basin).
3. The effect of restructuring during rifting and associated faulting on sediment transport and facies (Gawthorpe & Leeder, 2000; Leeder & Jackson, 1993). Rifting in southern Australia led to the exclusion of continental interior (Musgrave-derived) sediments in the post-rift sediments analysed. Instead, more localised sediment sourcing occurred from rift-exposed basement, and reworking of novel rift-associated sediment reservoirs. These findings further support observations on the importance of relative position within the rift basin for sediment provenance (Olierook et al., 2019).
4. The ultimate complete progression of a rift to a new ocean (Corti, 2009), inevitably leading to the establishment of fully oceanic conditions and new currents that dictate the transport of material on shelves and coasts. The opening of the Southern Ocean sea-way and increasing influence of dominantly westerly swells and vestiges of the warm-water Leeuwin Current ultimately established an eastward-directed long-shore-drift conveyer of sediment along the southern margin (James, Bone, Collins, & Kurtis Kyser, 2001; Pearce, Hart, Murphy, & Rice, 2015). The importance of this new transport system is expressed in the appearance of Albany–Fraser Orogen and Leeuwin Complex derived zircon grains in Plio-Pleistocene sediment of the Nundroo Plain, which originated from coastally exposed basement hundreds of kilometres to the west.

Collectively, rifting is, at least in part, manifest in the sediment record by (i) isolation of previous source regions as a consequence of intermediate sediment traps and development of cover, (ii) restructuring of sediment supply and reworking associated with differential uplift, faulting and basin compartmentalisation, *and* (iii) remodelled sediment transport dictated by transition to marine conditions, ocean currents and coastal erosion.

CONCLUSIONS

Comparison of post-rift detrital zircon populations from Australia's southern margin with existing pre- and syn-rift datasets, indicates a significant reorganisation of sediment routing beginning in the Cenozoic on the southern margin of Australia. This reorganisation coincided with the opening of the sea-way between Australia and Antarctica. During the Phanerozoic, a relatively stable zircon source and reworking system developed in central southern Australia as indicated by similar characteristic Proterozoic grains occurring throughout parts of the Officer Basin, the Madura Shelf and fringing Eocene and Miocene shorelines. Aridity and karstification reduced run-off and clastic input from continental areas adjacent to the modern southern margin during the Cenozoic, while highstands and carbonate blanketing effectively isolated sediment reservoirs of clastics and prevented reworking of the long-lived sediment pool characterising onshore pre- and syn-rift sequences. New sediment pathways activated at this time as local basement sources became dominant in the post-rift sediment samples, with the Moodini Supersuite of the underlying Coompana and Madura Provinces identified as a primary source. This material was likely derived from footwall fault scarps and an extensive region interpreted to have elevated crystalline basement. Furthermore, distinct age and Hf-isotope signatures within the ODP1126 sample demonstrates that grains with an east-coast detrital zircon signature were delivered further west during inversion and reworking from the Ceduna Sub-basin. Later, opening of Southern Ocean and development of east-directed long-shore drift and winds (during low-stands) has fundamentally altered the character of the sediment by input of long-distance sediment from the coastally available Leeuwin Complex and Albany–Fraser Orogen in southwestern Australia.

Processes associated with rifting (fault-scarp generation, inversion, basin subsidence, transition to marine influence, etc.) combine to alter regions of primary denudation, drive isolation of pre-existing sediment reservoirs and open up new transport pathways. Wholesale reorganisation of sediment systems is a natural consequence of rifting and such reorganisation can be resolved in the evolution of heavy mineral provenance.

DATA AVAILABILITY STATEMENT

The data that support the findings of this study are openly available in the supplementary material, as indicated throughout the text, at [URL], reference number [reference number].

REFERENCES

Aitken, A. R. A., Young, D. A., Ferraccioli, F., Betts, P. G., Greenbaum, J. S., Richter, T. G., . . . Siegert, M. J. (2014). The subglacial geology of Wilkes Land, East Antarctica. *Geophysical Research Letters, 41*(7), 2390-2400. doi:doi:10.1002/2014GL059405

Armitage, J. J., Duller, R. A., Whittaker, A. C., & Allen, P. A. (2011). Transformation of tectonic and climatic signals from source to sedimentary archive. *Nature Geosci, 4*(4), 231-235. doi:http://www.nature.com/ngeo/journal/v4/n4/abs/ngeo1087.html#supplementary-information

Ball, P., Eagles, G., Ebinger, C., McClay, K., & Totterdell, J. (2013). The spatial and temporal evolution of strain during the separation of Australia and Antarctica. *Geochemistry, Geophysics, Geosystems, 14*(8), 2771-2799. doi:10.1002/ggge.20160

Barham, M., Kirkland, C. L., & Danišík, M. (2019a). Assessing volcanic origins within detrital zircon populations – a case study from the Mesozoic non-volcanic margin of southern Australia. *Geoscience Frontiers*. doi:10.1016/j.gsf.2019.01.003

Barham, M., Kirkland, C. L., & Hollis, J. (2019b). Spot the difference: Zircon disparity tracks crustal evolution. *Geology, 47*(5), 435-439. doi:10.1130/G45840.1

Barham, M., Kirkland, C. L., Reynolds, S., O'Leary, M. J., Evans, N. J., Allen, H., . . . Goodall, J. (2016). The answers are blowin' in the wind: Ultra-distal ashfall zircons, indicators of Cretaceous super-eruptions in eastern Gondwana. *Geology, 44*(8), 643-646. doi:10.1130/g38000.1

Barham, M., Reynolds, S., Kirkland, C. L., O'Leary, M. J., Evans, N. J., Allen, H. J., . . . McDonald, B. J. (2018). Sediment routing and basin evolution in Proterozoic to Mesozoic east Gondwana: A case study from southern Australia. *Gondwana Research, 58*, 122-140. doi:https://doi.org/10.1016/j.gr.2018.03.006

Barnett-Moore, N., Flament, N., Heine, C., Butterworth, N., & Müller, R. D. (2014). Cenozoic uplift of south Western Australia as constrained by river profiles. *Tectonophysics, 622*, 186-197. doi:http://dx.doi.org/10.1016/j.tecto.2014.03.010

Bein, J., & Taylor, M. L. (1981). The Eyre Sub-basin: Recent exploration results. *APEA Journal, 21*(1), 91-98.

Belousova, E., Griffin, W., O'Reilly, S. Y., & Fisher, N. (2002). Igneous zircon: trace element composition as an indicator of source rock type. *Contributions to Mineralogy and Petrology, 143*(5), 602-622. doi:10.1007/s00410-002-0364-7

Belousova, E. A., Reid, A. J., Griffin, W. L., & O'Reilly, S. Y. (2009). Rejuvenation vs. recycling of Archean crust in the Gawler Craton, South Australia: Evidence from U–Pb and Hf isotopes in detrital zircon. *Lithos, 113*(3–4), 570-582. doi:http://dx.doi.org/10.1016/j.lithos.2009.06.028

Bendall, B., Jensen-Schmidt, B., Holford, S., Dutch, R., & Pawley, M. (2016). *Insights into the nature and extent of sedimentary basins underlying the Eucla Basin from reprocessing and interpretation of the 13GA-EG1 Eucla-Gawler Seismic Survey*. Paper presented at the Australian Earth Sciences Convention, Adelaide, South Australia.

Betts, P. G., & Giles, D. (2006). The 1800–1100Ma tectonic evolution of Australia. *Precambrian Research, 144*(1), 92-125. doi:https://doi.org/10.1016/j.precamres.2005.11.006

Black, L. P., Kamo, S. L., Allen, C. M., Davis, D. W., Aleinikoff, J. N., Valley, J. W., . . . Foudoulis, C. (2004). Improved $^{206}Pb/^{238}U$ microprobe geochronology by the monitoring of a trace-element-related matrix effect; SHRIMP, ID–TIMS, ELA–ICP–MS and oxygen isotope documentation for a series of zircon standards. *Chemical Geology, 205*(1), 115-140. doi:https://doi.org/10.1016/j.chemgeo.2004.01.003

Blakey, R. C. (2008). Gondwana paleogeography from assembly to breakup - A 500 m.y. odyssey. In C. R. Fielding, T. D. Frank, & J. L. Isbell (Eds.), *Resolving the Late Paleozoic Ice Age in Time and Space* (pp. 1-28). Boulder, Colorado: The Geological Society of America, Special Paper 441.

Blatt, H., & Jones, R. L. (1975). Proportions of Exposed Igneous, Metamorphic, and Sedimentary Rocks. *GSA Bulletin, 86*(8), 1085-1088. doi:10.1130/0016-7606(1975)86<1085:POEIMA>2.0.CO;2

Blevin, J. E., & Cathro, D. L. (2008). *Australian Southern Margin Synthesis, Project GA707*. Retrieved from

Blichert-Toft, J., & Albarède, F. (1997). The Lu-Hf isotope geochemistry of chondrites and the evolution of the mantle-crust system. *Earth and Planetary Science Letters, 148*(1–2), 243-258. doi:http://dx.doi.org/10.1016/S0012-821X(97)00040-X

Bodorkos, S., Love, G. J., Nelson, D. R., & Wingate, M. T. D. (2006). 149695: quartz sandstone, Quadrio Lake; Geochronology dataset 616. In *Compilation of geochronology data, June 2006 update*: Western Australia Geological Survey.

Boger, S. D. (2011). Antarctica — Before and after Gondwana. *Gondwana Research, 19*(2), 335-371. doi:https://doi.org/10.1016/j.gr.2010.09.003

Bradshaw, B. E., Rollet, N., Totterdell, J. M., & Borissova, I. (2003). A revised structural framework for frontier basins on the Southern and Southwestern Australian Continental Margin. *Geoscience Australia, Record 2003/03*, 1-94.

Bryan, S. E., Constantine, A. E., Stephens, C. J., Ewart, A., Schön, R. W., & Parianos, J. (1997). Early Cretaceous volcano-sedimentary successions along the eastern Australian continental margin: Implications for the break-up of eastern Gondwana. *Earth and Planetary Science Letters, 153*(1-2), 85-102.

Bryan, S. E., Cook, A. G., Allen, C. M., Siegel, C., Purdy, D. J., Greentree, J. S., & Uysal, I. T. (2012). Early-mid cretaceous tectonic evolution of eastern Gondwana: From silicic LIP magmatism to continental rupture. *Episodes, 35*(1), 142-152.

Camacho, A., Hensen, B. J., & Armstrong, R. (2002). Isotopic test of a thermally driven intraplate orogenic model, Australia. *Geology, 30*(10), 887-890. doi:10.1130/0091-7613(2002)030<0887:ITOATD>2.0.CO;2

Cawood, P. A., Hawkesworth, C. J., & Dhuime, B. (2012). Detrital zircon record and tectonic setting. *Geology, 40*(10), 875-878. doi:10.1130/g32945.1

Cawood, P. A., & Korsch, R. J. (2008). Assembling Australia: Proterozoic building of a continent. *Precambrian Research, 166*(1–4), 1-35. doi:http://dx.doi.org/10.1016/j.precamres.2008.08.006

Cawood, P. A., & Nemchin, A. A. (2000). Provenance record of a rift basin: U/Pb ages of detrital zircons from the Perth Basin, Western Australia. *Sedimentary Geology, 134*(3–4), 209-234. doi:http://dx.doi.org/10.1016/S0037-0738(00)00044-0

Cawood, P. A., Nemchin, A. A., Freeman, M., & Sircombe, K. (2003). Linking source and sedimentary basin: Detrital zircon record of sediment flux along a modern river system and implications for provenance studies. *Earth and Planetary Science Letters, 210*(1–2), 259-268. doi:http://dx.doi.org/10.1016/S0012-821X(03)00122-5

Collins, A. S. (2003). Structure and age of the northern Leeuwin Complex, Western Australia: constraints from field mapping and U–Pb isotopic analysis. *Australian Journal of Earth Sciences, 50*(4), 585-599. doi:10.1046/j.1440-0952.2003.01014.x

Corti, G. (2009). Continental rift evolution: From rift initiation to incipient break-up in the Main Ethiopian Rift, East Africa. *Earth-Science Reviews, 96*(1), 1-53. doi:https://doi.org/10.1016/j.earscirev.2009.06.005

de Broekert, P., & Sandiford, M. (2005). Buried inset-valleys in the eastern Yilgarn Craton, Western Australia: geomorphology, age, and allogenic control. *The Journal of Geology, 113*(4), 471-493. doi:doi:10.1086/430244

Direen, N. G., Borissova, I., Stagg, H. M. J., Colwell, J. B., & Symonds, P. A. (2007). Nature of the continent–ocean transition zone along the southern Australian continental margin: a comparison of the Naturaliste Plateau, SW Australia, and the central Great Australian Bight sectors. *Geological Society, London, Special Publications, 282*(1), 239-263. doi:10.1144/sp282.12

Direen, N. G., Stagg, H. M. J., Symonds, P. A., & Colwell, J. B. (2011). Dominant symmetry of a conjugate southern Australian and East Antarctic magma-poor rifted margin segment. *Geochemistry, Geophysics, Geosystems, 12*(2). doi:doi:10.1029/2010GC003306

Espurt, N., Callot, J.-P., Roure, F., Totterdell, J. M., Struckmeyer, H. I. M., & Vially, R. (2012). Transition from symmetry to asymmetry during continental rifting: an example from the Bight Basin–Terre Adélie (Australian and Antarctic conjugate margins). *Terra Nova, 24*(3), 167-180. doi:10.1111/j.1365-3121.2011.01055.x

Espurt, N., Callot, J.-P., Totterdell, J., Struckmeyer, H., & Vially, R. (2009). Interactions between continental breakup dynamics and large-scale delta system evolution: Insights from the Cretaceous Ceduna delta system, Bight Basin, Southern Australian margin. *Tectonics, 28*(6). doi:10.1029/2009TC002447

Feary, D. A., Hine, A. C., James, N. P., & Malone, M. J. (2004). Leg 182 synthesis: exposed secrets of the Great Australian Bight. In A. C. Hine, D. A. Feary, & M. J. Malone (Eds.), *Proceedings of the Ocean Drilling Program, Scientific Results* (Vol. 182, pp. 1-30).

Feary, D. A., Hine, A. C., & Malone, M. J. (1999). *Ocean Drilling Program Leg 182 preliminary report - Great Australian Bight: Cenozoic cool-water carbonates*: Texas A&M University.

Feary, D. A., & James, N. P. (1998). Seismic stratigraphy and geological evolution of the Cenozoic, cool-water Eucla Platform, Great Australian Bight. *AAPG Bulletin, 82*(5A), 792-816.

Fedo, C. M., Sircombe, K. N., & Rainbird, R. H. (2003). Detrital zircon analysis of the sedimentary record. *Reviews in Mineralogy and Geochemistry, 53*(1), 277-303. doi:10.2113/0530277

Fielding, L., Najman, Y., Millar, I., Butterworth, P., Ando, S., Padoan, M., . . . Kneller, B. (2017). A detrital record of the Nile River and its catchment. *Journal of the Geological Society, 174*(2), 301-317. doi:10.1144/jgs2016-075

Fitzsimons, I. C. W. (2003). Proterozoic basement provinces of southern and southwestern Australia, and their correlation with Antarctica. *Geological Society, London, Special Publications, 206*(1), 93-130. doi:10.1144/gsl.sp.2003.206.01.07

Fraser, G. L., & Neumann, N. L. (2016). *Under the Nullarbor: New SHRIMP UPb zircon ages from the Coompana, Madura and Albany-Fraser Provinces, and Officer Basin, western South Australia and eastern Western Australia: July 2014-June 2015*. Canberra: Record 2016/16. Geoscience Australia.

768 Gawthorpe, R. L., & Leeder, M. R. (2000). Tectono-sedimentary evolution of active extensional
769 basins. *Basin Research, 12*(3-4), 195-218. doi:doi:10.1111/j.1365-2117.2000.00121.x
770 Gehrels, G. E., Valencia, V. A., & Ruiz, J. (2008). Enhanced precision, accuracy, efficiency, and spatial
771 resolution of U-Pb ages by laser ablation–multicollector–inductively coupled plasma–mass
772 spectrometry. *Geochemistry, Geophysics, Geosystems, 9*(3), 1-13.
773 doi:10.1029/2007GC001805
774 Gibbons, A. D., Whittaker, J. M., & Müller, R. D. (2013). The breakup of East Gondwana: Assimilating
775 constraints from Cretaceous ocean basins around India into a best-fit tectonic model.
776 *Journal of Geophysical Research: Solid Earth, 118*(3), 808-822. doi:10.1002/jgrb.50079
777 Gibson, G. M., Totterdell, J. M., White, L. T., Mitchell, C. H., Stacey, A. R., Morse, M. P., & Whitaker,
778 A. (2013). Pre-existing basement structure and its influence on continental rifting and
779 fracture zone development along Australia's southern rifted margin. *Journal of the*
780 *Geological Society, 170*(2), 365. doi:10.1144/jgs2012-040
781 Grey, K., Hocking, R. H., Stevens, M. K., Bagas, L., Carlsen, G. M., Irimies, F., . . . Apak, S. N. (2005).
782 *Lithostratigraphic nomenclature of the Officer Basin and correlative parts of the Paterson*
783 *Orogen, Western Australia*: Geological Survey of Western Australia Report 93.
784 Griffin, W. L., Belousova, E. A., Shee, S. R., Pearson, N. J., & O'Reilly, S. Y. (2004). Archean crustal
785 evolution in the northern Yilgarn Craton: U–Pb and Hf-isotope evidence from detrital
786 zircons. *Precambrian Research, 131*(3–4), 231-282.
787 doi:http://dx.doi.org/10.1016/j.precamres.2003.12.011
788 Grimes, C. B., John, B. E., Kelemen, P. B., Mazdab, F. K., Wooden, J. L., Cheadle, M. J., . . . Schwartz, J.
789 J. (2007). Trace element chemistry of zircons from oceanic crust: A method for distinguishing
790 detrital zircon provenance. *Geology, 35*(7), 643-646. doi:10.1130/g23603a.1
791 Grimes, C. B., Wooden, J. L., Cheadle, M. J., & John, B. E. (2015). "Fingerprinting" tectono-magmatic
792 provenance using trace elements in igneous zircon. *Contributions to Mineralogy and*
793 *Petrology, 170*(5-6), 1-26. doi:10.1007/s00410-015-1199-3
794 Haines, P. W., Hocking, R. M., Grey, K., & Stevens, M. K. (2008). Vines 1 revisited: are older
795 Neoproterozoic glacial deposits preserved in Western Australia? *Australian Journal of Earth*
796 *Sciences, 55*(3), 397-406. doi:10.1080/08120090701769506
797 Haines, P. W., Kirkland, C. L., Wingate, M. T. D., Allen, H., Belousova, E. A., & Gréau, Y. (2016).
798 Tracking sediment dispersal during orogenesis: A zircon age and Hf isotope study from the
799 western Amadeus Basin, Australia. *Gondwana Research, 37*, 324-347.
800 doi:http://dx.doi.org/10.1016/j.gr.2015.08.011
801 Haines, P. W., Wingate, M. T. D., & Kirkland, C. L. (2013). Detrital Zircon U–Pb ages from the
802 Paleozoic of the Canning and Officer Basins, Western Australia: implications for provenance
803 and interbasin connections. *Proceedings of the West Australian Basins Symposium,*
804 *sponsored by the Western Australian Branch of the Petroleum Exploration Society of*
805 *Australia, Perth*, 1-19.
806 Hawkesworth, C. J., & Kemp, A. I. S. (2006). Using hafnium and oxygen isotopes in zircons to unravel
807 the record of crustal evolution. *Chemical Geology, 226*(3–4), 144-162.
808 doi:http://dx.doi.org/10.1016/j.chemgeo.2005.09.018
809 Holford, S. P., Tuitt, A. K., Hillis, R. R., Green, P. F., Stoker, M. S., Duddy, I. R., . . . Tassone, D. R.
810 (2014). Cenozoic deformation in the Otway Basin, southern Australian margin: implications
811 for the origin and nature of post-breakup compression at rifted margins. *Basin Research, 26*,
812 10-37. doi:10.1111/bre.12035
813 Hou, B., Alley, N. F., Frakes, L. A., Stoian, L., & Cowley, W. M. (2006). Eocene stratigraphic succession
814 in the Eucla Basin of South Australia and correlation to major regional sea-level events.
815 *Sedimentary Geology, 183*(3-4), 297-319.
816 Hou, B., Keeling, J., Reid, A., Fairclough, M., Wairland, I., Belousova, E., . . . Hocking, R. (2011). Heavy
817 mineral sands in the Eucla Basin, Southern Australia: depositional and province-scale
818 prospectivity. *Economic Geology, 106*, 687-712.

Huston, D. L., Blewett, R. S., & Champion, D. C. (2012). Australia through time: a summary of its tectonic and metallogenic evolution. *Episodes, 35*(1), 23-43.

Jackson, S. E., Pearson, N. J., Griffin, W. L., & Belousova, E. A. (2004). The application of laser ablation-inductively coupled plasma-mass spectrometry to in situ U–Pb zircon geochronology. *Chemical Geology, 211*(1–2), 47-69. doi:http://dx.doi.org/10.1016/j.chemgeo.2004.06.017

James, N. P., & Bone, Y. (2007). A late Pliocene–early Pleistocene, inner-shelf, subtropical, seagrass-dominated carbonate: Roe Calcarenite, Great Australian Bight, Western Australia. *Palaios, 22*(4), 343-359. doi:10.2110/palo.2005.p05-117r

James, N. P., Bone, Y., Collins, L. B., & Kurtis Kyser, T. (2001). Surficial sediments of the great australian bight: facies dynamics and oceanography on a vast cool-water carbonate shelf. *Journal of Sedimentary Research, 71*(4), 549-567.

James, N. P., Feary, D. A., Betzler, C., Bone, Y., Holbourn, A. E., Li, Q., . . . Surlyk, F. (2004). Origin of Late Pleistocene Bryozoan Reef Mounds; Great Australian Bight. *Journal of Sedimentary Research, 74*(1), 20-48. doi:10.1306/062303740020

JNOC. (1992). *Geological and geophysical study in offshore Eucla Basins, Western Australia*. Retrieved from Tokyo, Japan:

Johnson, S. P. (2013). *The birth of supercontinents and the Proterozoic assembly of Western Australia*: Geological Survey of Western Australia.

Kirkland, C. L., Smithies, R. H., & Spaggiari, C. V. (2015). Foreign contemporaries – Unravelling disparate isotopic signatures from Mesoproterozoic Central and Western Australia. *Precambrian Research, 265*, 218-231. doi:http://dx.doi.org/10.1016/j.precamres.2014.12.001

Kirkland, C. L., Smithies, R. H., Spaggiari, C. V., Wingate, M. T. D., Quentin de Gromard, R., Clark, C., . . . Belousova, E. A. (2017). Proterozoic crustal evolution of the Eucla basement, Australia: Implications for destruction of oceanic crust during emergence of Nuna. *Lithos, 278–281*, 427-444. doi:https://doi.org/10.1016/j.lithos.2017.01.029

Kirkland, C. L., Smithies, R. H., Woodhouse, A. J., Howard, H. M., Wingate, M. T. D., Belousova, E. A., . . . Spaggiari, C. V. (2013). Constraints and deception in the isotopic record; the crustal evolution of the west Musgrave Province, central Australia. *Gondwana Research, 23*(2), 759-781. doi:http://dx.doi.org/10.1016/j.gr.2012.06.001

Kositcin, N. (2010a). *Geodynamic synthesis of the Gawler Craton and Curnamona Province* (Vol. 2010/27): Geoscience Australia Record.

Kositcin, N. (2010b). *Geodynamic Synthesis of the Gawler Craton and Curnamona Province*: Geoscience Australia, Record, 2010/27.

Krassay, A. A., & Totterdell, J. M. (2003). Seismic stratigraphy of a large, Cretaceous shelf-margin delta complex, offshore southern Australia. *AAPG Bulletin, 87*(6), 935-963. doi:10.1306/01240300015

Lambiase, J. J., Morley, C. K., White, R. S., Watts, A. B., Bowler, D., Holroyd, R., & Kusznir, N. (1999). Hydrocarbons in Rift Basins: The Role of Stratigraphy [and Discussion]. *Philosophical Transactions: Mathematical, Physical and Engineering Sciences, 357*(1753), 877-900.

Leeder, M. R., & Jackson, J. A. (1993). The interaction between normal faulting and drainage in active extensional basins, with examples from the western United States and central Greece. *Basin Research, 5*(2), 79-102. doi:10.1111/j.1365-2117.1993.tb00059.x

Li, Q., James, N. P., & McGowran, B. (2003). Middle and Late Eocene Great Australian Bight lithobiostratigraphy and stepwise evolution of the southern Australian continental margin. *Australian Journal of Earth Sciences, 50*(1), 113-128. doi:10.1046/j.1440-0952.2003.00978.x

Lloyd, J., Collins, A. S., Payne, J. L., Glorie, S., Holford, S., & Reid, A. J. (2016). Tracking the Cretaceous transcontinental Ceduna River through Australia: The hafnium isotope record of detrital zircons from offshore southern Australia. *Geoscience Frontiers, 7*(2), 237-244. doi:http://dx.doi.org/10.1016/j.gsf.2015.06.001

Lowry, D. C. (1970). *Geology of the Western Australian part of the Eucla Basin*. (Bulletin 122). Perth: Geological Survey of Western Australia.

Ludwig, K. R. (1998). On the Treatment of Concordant Uranium-Lead Ages. *Geochimica et Cosmochimica Acta, 62*(4), 665-676. doi:https://doi.org/10.1016/S0016-7037(98)00059-3

Ludwig, K. R. (2012). *User's Manual for Isoplot/Ex, v.3.75, A Geochronological Toolkit for Microsoft Excel*: Berkeley Geochronological Center Special Publications, 5.

Macdonald, J., Backé, G., King, R., Holford, S., & Hillis, R. (2012). Geomechanical modelling of fault reactivation in the Ceduna Sub-basin, Bight Basin, Australia. *Geological Society, London, Special Publications, 367*(1), 71. doi:10.1144/SP367.6

MacDonald, J. D., Holford, S. P., Green, P. F., Duddy, I. R., King, R. C., & Backé, G. (2013). Detrital zircon data reveal the origin of Australia's largest delta system. *Journal of the Geological Society, 170*(1), 3-6. doi:10.1144/jgs2012-093

Makulini, P., Kirkland, C. L., & Barham, M. (2018). Zircon grain shape holds provenance information; a case study from southwestern Australia. *Geological Journal*, 1-15.

Mann, P., Gahagan, L., & Gordon, M. B. (2003). Tectonic setting of the World's giant oil and gas fields. In M. T. Halbouty (Ed.), *Giant oil and gas fields in the decade 19990-1999* (pp. 15-105): AAPG Memoir 78.

Markwitz, V., Kirkland, C. L., & Evans, N. J. (2016). Early Cambrian metamorphic zircon in the northern Pinjarra Orogen: Implications for the structure of the West Australian Craton margin. *Lithosphere*. doi:10.1130/l569.1

Mason, C. C., Fildani, A., Gerber, T., Blum, M. D., Clark, J. D., & Dykstra, M. (2017). Climatic and anthropogenic influences on sediment mixing in the Mississippi source-to-sink system using detrital zircons: Late Pleistocene to recent. *Earth and Planetary Science Letters, 466*, 70-79. doi:http://dx.doi.org/10.1016/j.epsl.2017.03.001

Meeuws, F. J. E., Holford, S. P., Foden, J. D., & Schofield, N. (2016). Distribution, chronology and causes of Cretaceous – Cenozoic magmatism along the magma-poor rifted southern Australian margin: Links between mantle melting and basin formation. *Marine and Petroleum Geology, 73*, 271-298. doi:https://doi.org/10.1016/j.marpetgeo.2016.03.003

Mole, D. R., Fiorentini, M. L., Cassidy, K. F., Kirkland, C. L., Thebaud, N., McCuaig, T. C., . . . Miller, J. (2013). Crustal evolution, intra-cratonic architecture and the metallogeny of an Archaean craton. *Geological Society, London, Special Publications, 393*. doi:10.1144/sp393.8

Mole, D. R., Fiorentini, M. L., Thebaud, N., Cassidy, K. F., McCuaig, T. C., Kirkland, C. L., . . . Miller, J. (2014). Archean komatiite volcanism controlled by the evolution of early continents. *Proceedings of the National Academy of Sciences, 111*(28), 10083.

Morel, M. L. A., Nebel, O., Nebel-Jacobsen, Y. J., Miller, J. S., & Vroon, P. Z. (2008). Hafnium isotope characterization of the GJ-1 zircon reference material by solution and laser-ablation MC-ICPMS. *Chemical Geology, 255*(1), 231-235. doi:https://doi.org/10.1016/j.chemgeo.2008.06.040

Morón, S., Cawood, P. A., Haines, P. W., Gallagher, S. J., Zahirovic, S., Lewis, C. J., & Moresi, L. (2019). Long-lived transcontinental sediment transport pathways of East Gondwana. *Geology, 47*(6), 513-516. doi:10.1130/G45915.1

Morrissey, L. J., Hand, M., & Kelsey, D. E. (2017a). A curious case of agreement between conventional thermobarometry and phase equilibria modelling in granulites: New constraints on P–T estimates in the Antarctica segment of the Musgrave–Albany–Fraser–Wilkes Orogen. *Journal of Metamorphic Geology, 35*(9), 1023-1050. doi:10.1111/jmg.12266

Morrissey, L. J., Payne, J. L., Hand, M., Clark, C., Taylor, R., Kirkland, C. L., & Kylander-Clark, A. (2017b). Linking the Windmill Islands, east Antarctica and the Albany–Fraser Orogen: Insights from U–Pb zircon geochronology and Hf isotopes. *Precambrian Research, 293*, 131-149. doi:https://doi.org/10.1016/j.precamres.2017.03.005

Müller, R. D., Flament, N., Matthews, K. J., Williams, S. E., & Gurnis, M. (2016). Formation of Australian continental margin highlands driven by plate–mantle interaction. *Earth and Planetary Science Letters, 441*, 60-70. doi:http://dx.doi.org/10.1016/j.epsl.2016.02.025

Nelson, D. R. (1997). Evolution of the Archaean granite-greenstone terranes of the Eastern Goldfields, Western Australia: SHRIMP U-Pb zircon constraints. *Precambrian Research, 83*(1), 57-81. doi:http://dx.doi.org/10.1016/S0301-9268(97)00005-3

Nelson, D. R. (1999). 154109: quartz-carbonate diamictite, Empress 1A. In *Compilation of geochronology data, 1998* (pp. 190-193): Western Australia Geological Survey, Record 1999/2.

Nelson, D. R. (2002a). 154880: sandstone, Pirrilyungka Outstation; Geochronology dataset 259. In *Compilation of geochronology data, June 2006 update*: Western Australia Geological Survey.

Nelson, D. R. (2002b). 154881: sandstone, Pirrilyungka Outstation; Geochronology dataset 260. In *Compilation of geochronology data, June 2006 update*: Western Australia Geological Survey.

Nelson, D. R. (2004a). 154666: arenite, Empress 1A; Geochronology dataset 52. In *Compilation of geochronology data, June 2006 update*: Western Australia Geological Survey.

Nelson, D. R. (2004b). 154667: sandstone, Empress 1A; Geochronology dataset 258. In *Compilation of geochronology data, June 2006 update*: Western Australia Geological Survey.

Nelson, D. R. (2004c). 154668: sandstone, Empress 1A; Geochronology dataset 53. In *Compilation of geochronology data, June 2006 update*: Western Australia Geological Survey.

Neumann, N. L., & Fraser, G. L. (2016). Under the Nullarbor: New SHRIMP U-Pb zircon ages from the Coompana, Madura and Albany-Fraser Provinces, and Officer Basin, western South Australia and eastern Western Australia. In: Commonwealth of Australia (Geoscience Australia).

Olierook, H. K. H., Barham, M., Fitzsimons, I. C. W., Timms, N. E., Jiang, Q., Evans, N. J., & McDonald, B. J. (2019). Tectonic controls on sediment provenance evolution in rift basins: detrital zircon U–Pb and Hf isotope analysis from the Perth Basin, Western Australia. *Gondwana Research, 66*, 126-142.

Paton, C., Hellstrom, J., Paul, B., Woodhead, J., & Hergt, J. (2011). Iolite: Freeware for the visualisation and processing of mass spectrometric data. *Journal of Analytical Atomic Spectrometry, 26*(12), 2508-2518. doi:10.1039/C1JA10172B

Payne, J. L., Hand, M., Barovich, K. M., Reid, A., & Evans, D. A. D. (2009). Correlations and reconstruction models for the 2500-1500 Ma evolution of the Mawson Continent. *Geological Society, London, Special Publications, 323*(1), 319-355. doi:10.1144/sp323.16

Pearce, A., Hart, A., Murphy, D., & Rice, H. (2015). *Seasonal wind patterns around the Western Australian coastline and their application in fisheries analysis*. Retrieved from Department of Fisheries, Western Australia:

Quigley, M. C., Clark, D., & Sandiford, M. (2010). Tectonic geomorphology of Australia. *Geological Society, London, Special Publications, 346*(1), 243-265. doi:10.1144/sp346.13

Reid, A., Keeling, J., Boyd, D., Belousova, E., & Hou, B. (2013). Source of zircon in world-class heavy mineral placer deposits of the Cenozoic Eucla Basin, southern Australia from LA-ICPMS U–Pb geochronology. *Sedimentary Geology, 286–287*, 1-19. doi:http://dx.doi.org/10.1016/j.sedgeo.2012.10.008

Requilme, L. (2016). *Detrital Mineral Assemblage Analysis of Modern and Ancient Shorelines from Western Australia.* (BSc (Hons.)), Curtin University,

Roberts, N. M. W., & Spencer, C. J. (2015). The zircon archive of continent formation through time. *Geological Society, London, Special Publications, 389*(1), 197-225. doi:10.1144/sp389.14

Ronov, A. B., Khain, V. E., Balukhovsky, A. N., & Seslavinsky, K. B. (1980). Quantitative analysis of Phanerozoic sedimentation. *Sedimentary Geology, 25*(4), 311-325. doi:https://doi.org/10.1016/0037-0738(80)90067-6

Rovere, A., Raymo, M. E., Mitrovica, J. X., Hearty, P. J., O'Leary, M. J., & Inglis, J. D. (2014). The Mid-Pliocene sea-level conundrum: Glacial isostasy, eustasy and dynamic topography. *Earth and Planetary Science Letters, 387*, 27-33. doi:http://dx.doi.org/10.1016/j.epsl.2013.10.030

970 Salles, T., Flament, N., & Müller, D. (2017). Influence of mantle flow on the drainage of eastern
971 Australia since the Jurassic Period. *Geochemistry, Geophysics, Geosystems, 18*(1), 280-305.
972 doi:10.1002/2016GC006617
973 Sandiford, M. (2007). The tilting continent: A new constraint on the dynamic topographic field from
974 Australia. *Earth and Planetary Science Letters, 261*(1–2), 152-163.
975 doi:http://dx.doi.org/10.1016/j.epsl.2007.06.023
976 Scherer, E., Münker, C., & Mezger, K. (2001). Calibration of the lutetium-hafnium clock. *Science,*
977 *293*(5530), 683-687. doi:10.1126/science.1061372
978 Seton, M., Müller, R. D., Zahirovic, S., Gaina, C., Torsvik, T., Shephard, G., . . . Chandler, M. (2012).
979 Global continental and ocean basin reconstructions since 200Ma. *Earth-Science Reviews,*
980 *113*(3), 212-270. doi:https://doi.org/10.1016/j.earscirev.2012.03.002
981 Shaanan, U., Rosenbaum, G., & Sihombing, F. M. H. (2017). Continuation of the Ross–Delamerian
982 Orogen: insights from eastern Australian detrital-zircon data. *Australian Journal of Earth*
983 *Sciences*, 1-9. doi:10.1080/08120099.2017.1354916
984 Sircombe, K. N., & Freeman, M. J. (1999). Provenance of detrital zircons on the Western Australia
985 coastline—Implications for the geologic history of the Perth basin and denudation of the
986 Yilgarn craton. *Geology, 27*(10), 879-882. doi:10.1130/0091-
987 7613(1999)027<0879:podzot>2.3.co;2
988 Spaggiari, C. V., Kirkland, C. L., Smithies, R. H., Wingate, M. T. D., & Belousova, E. A. (2015).
989 Transformation of an Archean craton margin during Proterozoic basin formation and
990 magmatism: The Albany–Fraser Orogen, Western Australia. *Precambrian Research, 266*, 440-
991 466. doi:http://dx.doi.org/10.1016/j.precamres.2015.05.036
992 Spaggiari, C. V., & Smithies, R. H. (2015). *Eucla basement stratigraphic drilling results release*
993 *workshop: extended abstracts*. Retrieved from
994 Stagg, H. M. J., Cockshell, C. D., Willcox, J. B., Hill, A. J., Needham, D. J. L., Thomas, B., . . . Hough, L. P.
995 (1990). *Basins of the Great Australian Bight region: geology and petroleum potential*: Bureau
996 of Mineral Resources, Continental Margins Program Folio 5.
997 Totterdell, J. M., Blevin, J. E., Struckmeyer, H. I. M., Bradshaw, B. E., Colwell, J. B., & Kennard, J. M.
998 (2000). A new sequence framework for the Great Australian Bight: starting with a clean
999 slate. *Australian Petroleum Production & Exploration Association, 40*, 95-117.
1000 Totterdell, J. M., & Bradshaw, B. E. (2004). The structural framework and tectonic evolution of the
1001 Bight Basin. In P. J. Boult, D. R. Johns, & S. C. Lang (Eds.), *Eastern Australasian Basins*
1002 *Symposium II* (pp. 41-61): Petroleum Exploration Society of Australia, Special Publication.
1003 Totterdell, J. M., & Krassay, A. A. (2003). *Sequence stratigraphic correlation of onshore and offshore*
1004 *Bight Basin successions*. Retrieved from
1005 Tucker, R. T. (2014). *Stratigraphy, sedimentation and age of the upper Cretaceous Winton Formation,*
1006 *central-western Queensland, Australia: implications for regional palaeogeography,*
1007 *palaeoenvironments and Gondwanan palaeontology.* (PhD), James Cook University,
1008 Tucker, R. T., Roberts, E. M., Henderson, R. A., & Kemp, A. I. S. (2016). Large igneous province or
1009 long-lived magmatic arc along the eastern margin of Australia during the Cretaceous?
1010 Insights from the sedimentary record. *Geological Society of America Bulletin, 128*(9-10),
1011 1461-1480. doi:10.1130/b31337.1
1012 Tucker, R. T., Roberts, E. M., Hu, Y., Kemp, A. I. S., & Salisbury, S. W. (2013). Detrital zircon age
1013 constraints for the Winton Formation, Queensland: Contextualizing Australia's Late
1014 Cretaceous dinosaur faunas. *Gondwana Research, 24*(2), 767-779.
1015 doi:http://dx.doi.org/10.1016/j.gr.2012.12.009
1016 Vavrek, M. J. (2016). The fragmentation of Pangaea and Mesozoic terrestrial vertebrate biodiversity.
1017 *Biology Letters, 12*(9), 20160528. doi:doi:10.1098/rsbl.2016.0528
1018 Veevers, J. J., Belousova, E. A., & Saeed, A. (2016). Zircons traced from the 700–500 Ma
1019 Transgondwanan Supermountains and the Gamburtsev Subglacial Mountains to the
1020 Ordovician Lachlan Orogen, Cretaceous Ceduna Delta, and modern Channel Country,

central-southern Australia. *Sedimentary Geology, 334*, 115-141. doi:http://dx.doi.org/10.1016/j.sedgeo.2016.01.014

Veevers, J. J., Saeed, A., Belousova, E. A., & Griffin, W. L. (2005). U–Pb ages and source composition by Hf-isotope and trace-element analysis of detrital zircons in Permian sandstone and modern sand from southwestern Australia and a review of the paleogeographical and denudational history of the Yilgarn Craton. *Earth-Science Reviews, 68*(3–4), 245-279. doi:http://dx.doi.org/10.1016/j.earscirev.2004.05.005

Vermeesch, P. (2004). How many grains are needed for a provenance study? *Earth and Planetary Science Letters, 224*(3), 441-451. doi:http://dx.doi.org/10.1016/j.epsl.2004.05.037

Vermeesch, P. (2012). On the visualisation of detrital age distributions. *Chemical Geology, 312-313*, 190-194. doi:https://doi.org/10.1016/j.chemgeo.2012.04.021

Vermeesch, P. (2018). Dissimilarity measures in detrital geochronology. *Earth-Science Reviews, 178*, 310-321. doi:https://doi.org/10.1016/j.earscirev.2017.11.027

Vermeesch, P., Resentini, A., & Garzanti, E. (2016). An R package for statistical provenance analysis. *Sedimentary Geology, 336*(Supplement C), 14-25. doi:https://doi.org/10.1016/j.sedgeo.2016.01.009

Walter, M. R., Veevers, J. J., Calver, C. R., & Grey, K. (1995). Neoproterozoic stratigraphy of the Centralian Superbasin, Australia. *Precambrian Research, 73*(1), 173-195. doi:http://dx.doi.org/10.1016/0301-9268(94)00077-5

Wiedenbeck, M., AllÉ, P., Corfu, F., Griffin, W. L., Meier, M., Oberli, F., . . . Spiegel, W. (1995). Three natural zircon standards for U-Th-Pb, Lu-Hf, trace element and REE analyses. *Geostandards Newsletter, 19*(1), 1-23. doi:10.1111/j.1751-908X.1995.tb00147.x

Willcox, J. B., & Stagg, H. M. J. (1990). Australia's southern margin: a product of oblique extension. *Tectonophysics, 173*(1), 269-281. doi:http://dx.doi.org/10.1016/0040-1951(90)90223-U

Wingate, M. T. D., & Bodorkos, S. (2007a). 181871: quartz sandstone, Lancer 1; Geochronology dataset 683. In *Compilation of geochronology data*: Western Australia Geological Survey.

Wingate, M. T. D., & Bodorkos, S. (2007b). 181872: quartz sandstone, Lancer 1; Geochronology dataset 684. In *Compilation of geochronology data*: Western Australia Geological Survey.

Wingate, M. T. D., & Bodorkos, S. (2007c). 181873: quartz sandstone, Lancer 1; Geochronology dataset 685. In *Compilation of geochronology data*: Western Australia Geological Survey.

Wingate, M. T. D., Kirkland, C. L., Haines, P. W., & Hocking, R. M. (2013). *199424: sandstone, Empress 1; Geochronology Record 1113*: Geological Survey of Western Australia.

Wingate, M. T. D., Kirkland, C. L., Spaggiari, C. V., & Smithies, R. H. (2015). U-Pb geochronology of the Madura Province. In C. V. Spaggiari & R. H. Smithies (Eds.), *Eucla basement stratigraphic drilling results release workshop: extended abstracts* (pp. 14-16): Geological Survey of Western Australia, Record 2015/10.

Woodhead, J. D., & Hergt, J. M. (2005). A Preliminary Appraisal of Seven Natural Zircon Reference Materials for In Situ Hf Isotope Determination. *Geostandards and Geoanalytical Research, 29*(2), 183-195. doi:10.1111/j.1751-908X.2005.tb00891.x

Xu, J., Snedden, J. W., Stockli, D. F., Fulthorpe, C. S., & Galloway, W. E. (2017). Early Miocene continental-scale sediment supply to the Gulf of Mexico Basin based on detrital zircon analysis. *Geological Society of America Bulletin, 129*(1-2), 3-22. doi:10.1130/b31465.1

1065 **TABLES**

1066

1067 *Table 1. Characteristic ages of zircon grains from relevant crystalline source regions of Australia.*
1068 *Italicised greyscale ages are less diagnostic of the element.*

Crustal element	Characteristic ages	References
Whitsunday Volcanic Province	Dominantly 130-95 Ma	Bryan et al. (2012)
New England Orogen	Dominantly 300-200 Ma	Shaanan, Rosenbaum, and Sihombing (2017); Veevers et al. (2016)
Lachlan Orogen	Dominantly 600-450 Ma	Shaanan et al. (2017); Veevers et al. (2016)
Leeuwin Complex (Pinjarra Orogen)	Dominant peaks at ~535, 690 Ma *~800-500 Ma, ~1200-1000 Ma*	Collins (2003)
Madura Province	Dominant peaks at ~1.15 Ga, ~1.4 Ga	Fraser and Neumann (2016); Kirkland et al. (2017)
Coompana Province	Dominant peaks at ~1.15 Ga, ~1.65 Ga	Fraser and Neumann (2016); Kirkland et al. (2017)
Albany-Fraser Orogen	Dominant peaks at ~1.2-1.1 Ga, ~1.7-1.6 Ga *~1.8-1.1 Ga*	Spaggiari et al. (2015)
Musgrave Orogen	Dominant peaks at ~1.1-1.0 Ga, ~1.25-1. 15 Ga, ~1.3 Ga, ~1.6-1.5 Ga,	Kirkland et al. (2015)
Gawler Craton	Dominant peaks at ~1.85-1.6 Ga, ~2.5 Ga	Kositcin (2010b)
Yilgarn Craton	Dominant peaks at ~2.8-2.6 Ga *~4.4-2.5 Ga*	Mole et al. (2013); Nelson (1997); Veevers et al. (2005)

1069

1070

Table 2. Sample age, location and stratigraphic position.

Expedition	*Site*	*Hole*	*Section*	*Top (cm)*	*Base (cm)*	*Latitude*	*Longitude*	*Sample #*	*Mass (g)*	*Age*
ODP-182	1126	D	28R-1	406.52	407.02	33° 30.5613'S	128° 03.9844'E	1126-2	677	Cretaceous-Eocene
ODP-182	1126	D	33R-1; 33R-2	454.85	455.35	33° 30.5613'S	128° 03.9844'E	1126-3	660	Cretaceous-Eocene
ODP-182	1128	D	6R-3	282.8	283.3	34° 23.4563'S	127° 35.4554'E	1128-1	530	Eocene
ODP-182	1128	D	23R-2; 23R-3	445.7	446.2	34° 23.4563'S	127° 35.4554'E	1128-2	630	Eocene
ODP-182	1130	C	8R-1	367.2	367.8	33° 25.1988'S	127° 36.1248'E	1130-1	709	Cretaceous-Eocene
ODP-182	1130	C	10R-1	385.95	386.45	33° 25.1988'S	127° 36.1248'E	1130-2	569	Cretaceous-Eocene
ODP-182	1134	A	41X-CC	368.2	368.5	33° 31.7244'S	127° 15.8400'E	1134-2	379	Eocene
Iluka onshore sample	Nundroo Plain	NDR-014	N/A	70.5 m	72 m	confidential	confidential	NDR014	~100	Plio-Pleistocene?

FIGURE CAPTIONS

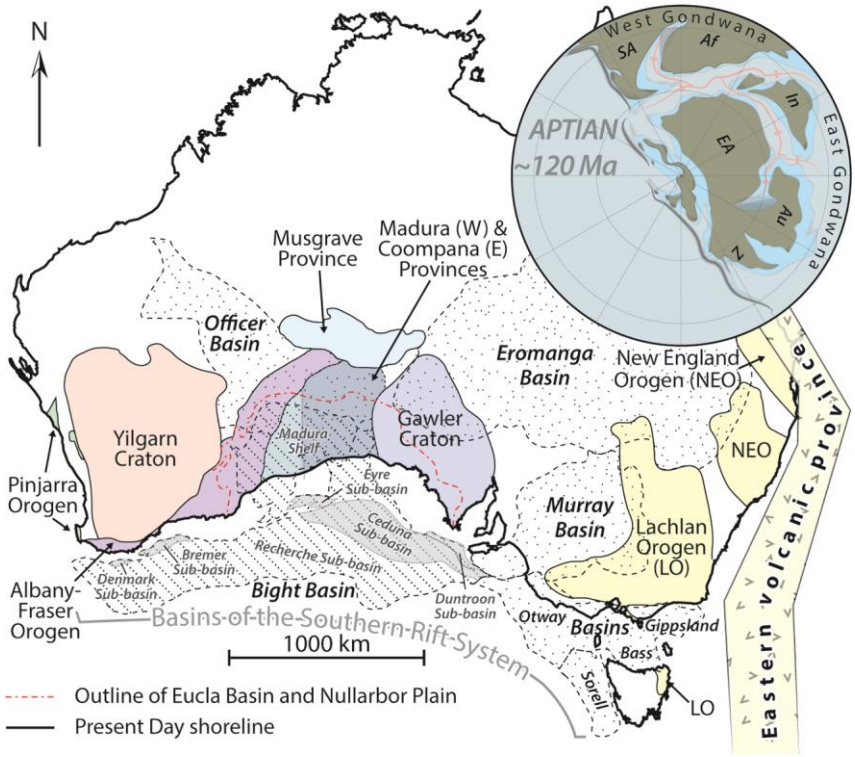

Figure 1. Geological map of the major crustal elements and sedimentary basins mentioned in the text. Inset map shows a palaeogeographic reconstruction for the middle-Cretaceous centred on the south pole, red lines correspond to spreading ridges, SA – South America, Af – Africa, In – India, EA – East Antarctica, Au – Australia, Z – Zealandia; modified from Blakey (2008). The main map is synthesised from multiple sources including Bryan et al. (1997), Totterdell and Bradshaw (2004), Blevin and Cathro (2008) and Barham et al. (2018).

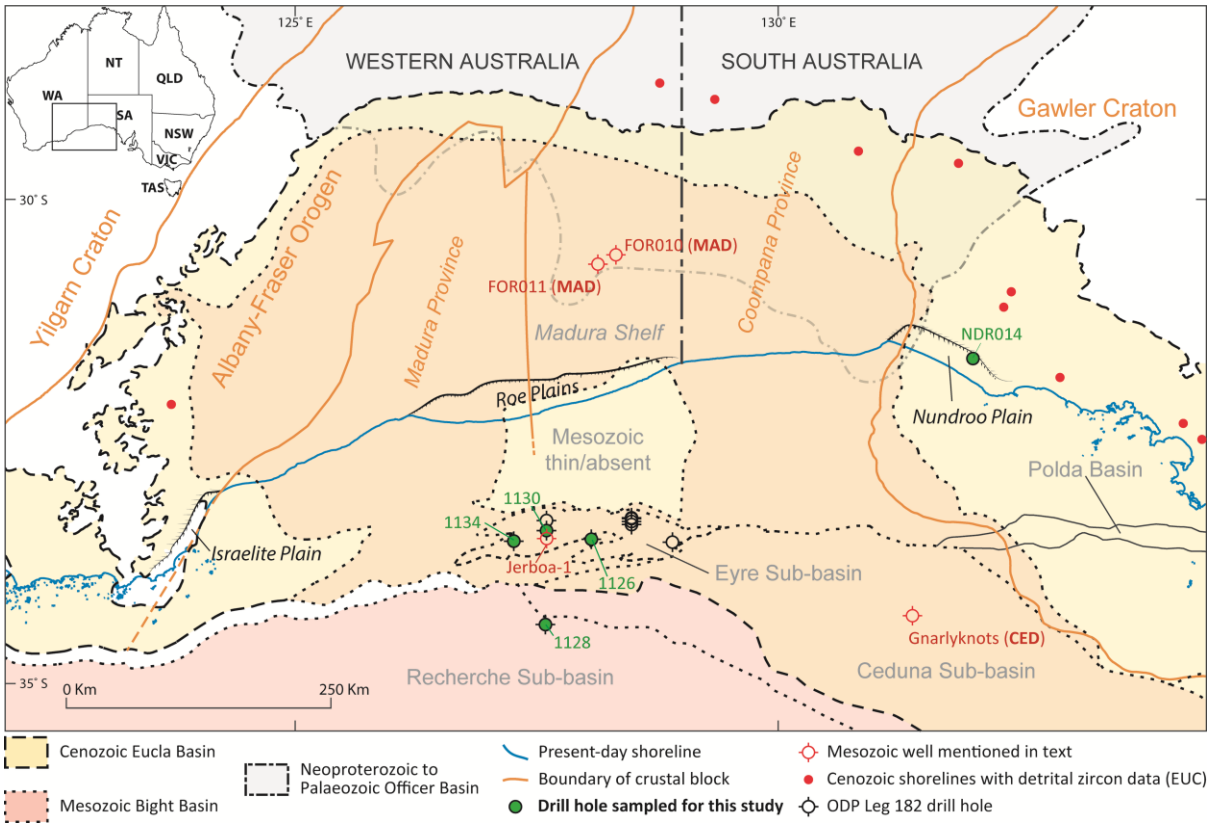

Figure 2. Geological and geographical map of the study region with smaller inset map showing the regions position with respect to Australia in general. Modified from Bradshaw et al. (2003).

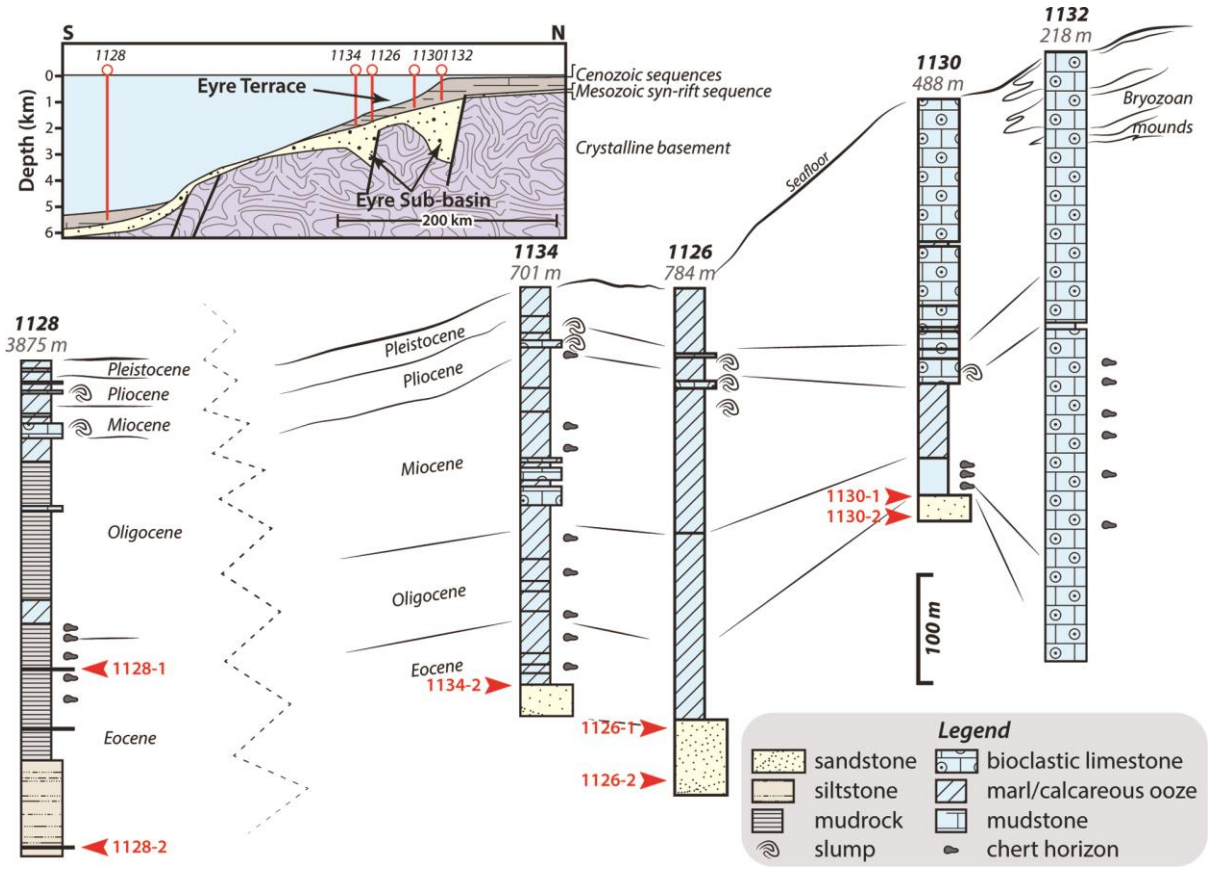

Figure 3. Simplified stratigraphical logs of the ODP drill transect sampled here. Red arrows and corresponding numbers refer to samples analysed, and referred to in the text. Modified from Feary et al. (1999).

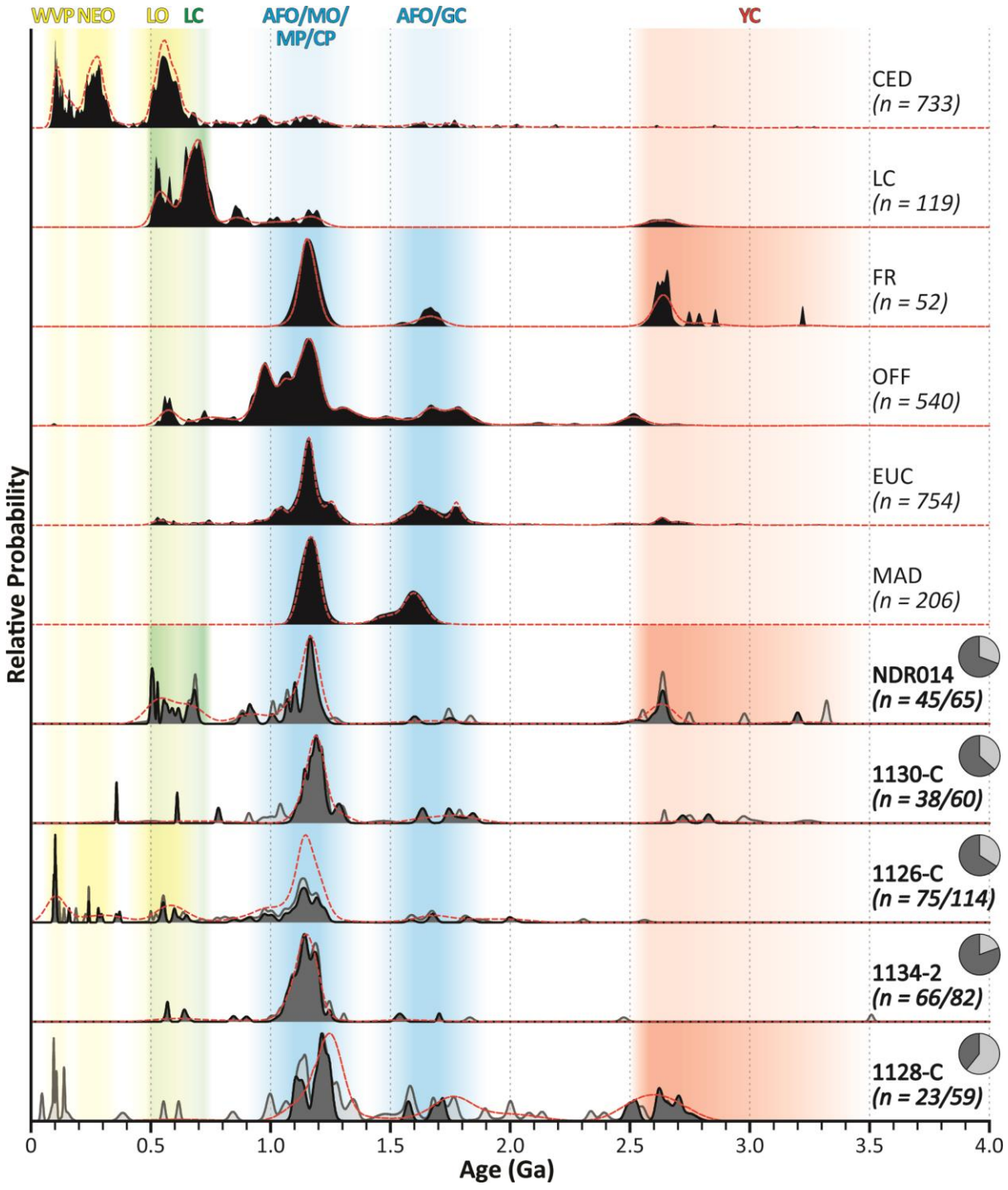

1093

1094 **Figure 4.** Stacked plots of detrital zircon age spectra. Red dashed lines represent kernel density
1095 estimates of data within 10% of concordia, grey fill areas represent standard probability density
1096 functions (light grey = all age data; dark grey = concordant data). Black-filled plots represent
1097 concordant data from published comparable detrital datasets. CED – Ceduna Delta in eastern Bight
1098 Basin (MacDonald et al., 2013), LC - Leeuwin Complex derived material (composite dataset from
1099 combined Yallingup and Augusta samples; Requilme, 2016; Sircombe & Freeman, 1999), FR –

Frankland River sediment draining the Albany-Fraser Orogen (FR3; Cawood et al., 2003), OFF – Officer Basin sediments (Bodorkos, Love, Nelson, & Wingate, 2006; Nelson, 1999, 2002a, 2002b, 2004a, 2004b, 2004c; Reid et al., 2013; Wingate & Bodorkos, 2007a, 2007b, 2007c; Wingate, Kirkland, Haines, & Hocking, 2013), EUC – Cenozoic shorelines fringing Eucla Basin (Reid et al., 2013), MAD – Madura Shelf polycyclic sediment (Barham et al., 2018). Coloured bars indicate significant age signatures of crystalline source regions. WVP – Whitsunday Volcanic Province, NEO – New England Orogen and LO – Lachlan Orogen, LC – Leeuwin Complex of the Pinjarra Orogen, AFO – Albany Fraser Orogen, MO – Musgrave Province (orogen), MP – Madura Province, CP – Coompana Province, GC – Gawler Craton, YC – Yilgarn Craton. Pie charts indicate the proportion of concordant analyses in each sample.

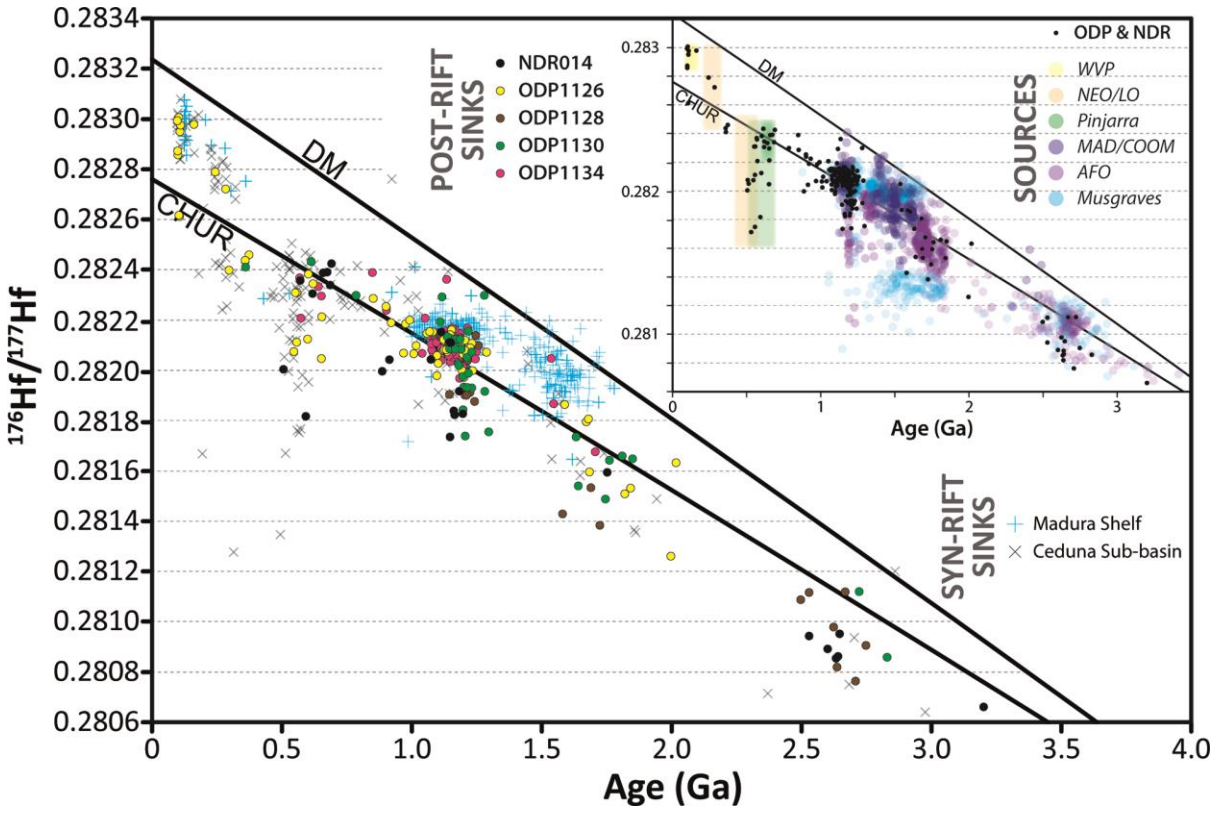

Figure 5. Hafnium-evolution plot of detrital zircon grains analysed from post-rift southern margin sediments overlain on older detrital and magmatic (inset) zircon data. Madura Shelf data from Barham et al. (2018), Ceduna Sub-basin data from Lloyd et al. (2016). Inset shows main post-rift detrital

populations with respect to the Hf-isotopic compositions of crystalline source regions – Musgrave Province data from Kirkland et al. (2015); AFO = Albany–Fraser Orogen from Spaggiari et al. (2015); MAD/COOM = Madura and Coompana Provinces from Kirkland et al. (2017); Pinjarra Orogen data from Veevers et al. (2005) and Olierook et al. (2019; and references therein); NEO/LO = New England Orogen and Lachlan Orogen from those compiled in Lloyd et al. (2016); WVP = Whitsunday Volcanic Province from Tucker (2014). Hafnium isotope values calculated at grain crystallisation age. Age uncertainty typically within data points as plotted and Hf-isotope uncertainty averages 0.000066 at 2σ. DM—depleted mantle; CHUR—chondritic uniform reservoir.

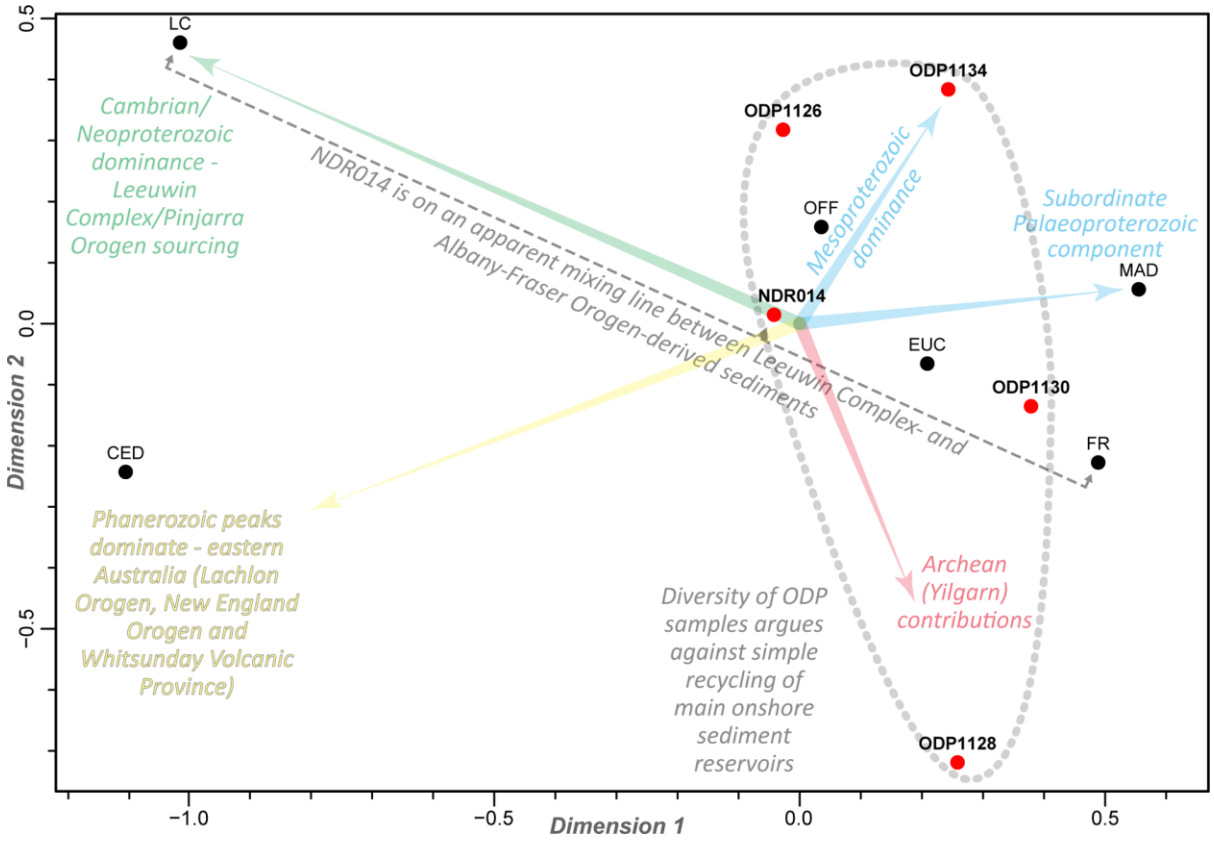

Figure 6. Kolmogorov–Smirnov based multi-dimensional-scaling plot of detrital zircon age spectra dissimilarities (Vermeesch, 2018). Samples that plot closer together have more similar detrital age populations, whereas those that are more dispersed have larger maximum differences calculated between their age spectra. Interpretations of the critical age peaks that cause sample differences (dispersion in MDS space) are shown. Black points refer to comparable sedimentary datasets. LC -

Leeuwin Complex derived material (composite dataset from combined Yallingup and Augusta samples; Requilme, 2016; Sircombe and Freeman, 1999), CED – Ceduna Delta in eastern Bight Basin (MacDonald et al., 2013), FR – Frankland River sediment draining the Albany-Fraser Orogen (FR3; Cawood et al., 2003), EB – Cenozoic shorelines fringing Eucla Basin (Reid et al., 2013), OFF – Officer Basin sediments (Bodorkos et al., 2006; Nelson, 1999, 2002a, b, 2004a, b, c; Reid et al., 2013; Wingate and Bodorkos, 2007a, b, c; Wingate et al., 2013), MAD – Madura Shelf polycyclic sediments (Barham et al., 2018).

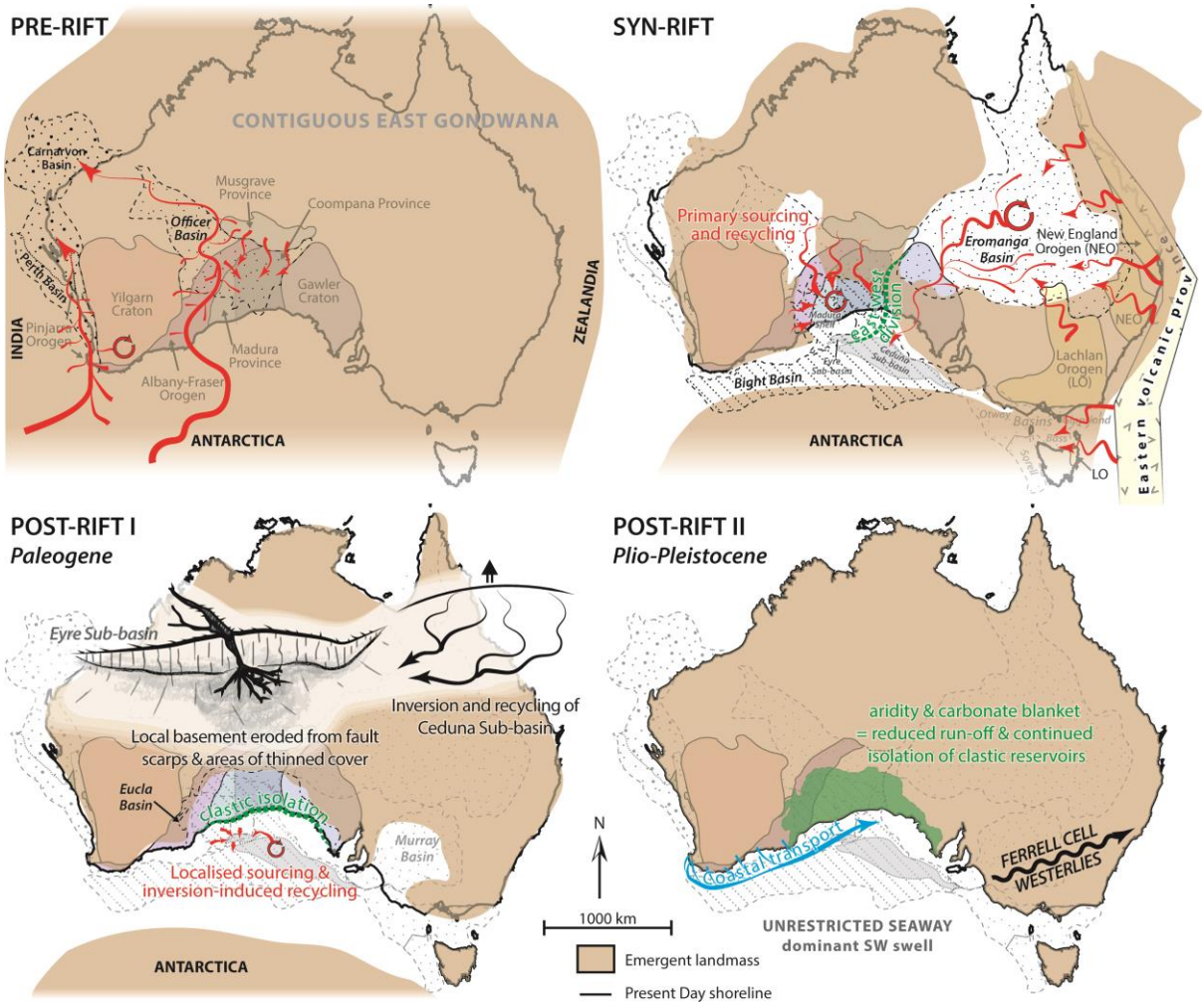

Figure 7. Schematic summary diagram showing the evolution of sediment routing for the southern margin of Australia (and relevant sediment reservoirs) across its rifting history. Note the rift stages refer specifically to the southern margin. Pre-rift taken as a composite of aspects of the Neoproterozoic and Palaeozoic (Barham et al., 2018; Haines et al., 2013; Haines et al., 2016; Morón

et al., 2019; Olierook et al., 2019). Syn-rift information derived from and Barham et al. (2018); Lloyd et al. (2016); Tucker et al. (2013); Veevers et al. (2016). Post-rift stages I and II based on this work.